Phosphoproteomics Profiling Defines a Target Landscape of the Basophilic Protein Kinases AKT, S6K, and RSK in Skeletal Myotubes

Fricke, Anna L.; Mühlhäuser, Wignand W.D.; Reimann, Lena; Zimmermann, Johannes P.; Reichenbach, Christa; Knapp, Bettina; Peikert, Christian D.; Heberle, Alexander M.; Faessler, Erik; Schäuble, Sascha

Published in:
Journal of Proteome Research

DOI:
10.1021/acs.jproteome.2c00505

Publication date:
2023

Journal of proteome research

pubs.acs.org/jpr Article

Phosphoproteomics Profiling Defines a Target Landscape of the Basophilic Protein Kinases AKT, S6K, and RSK in Skeletal Myotubes

Anna L. Fricke, Wignand W. D. Mühlhäuser, Lena Reimann, Johannes P. Zimmermann, Christa Reichenbach, Bettina Knapp, Christian D. Peikert, Alexander M. Heberle, Erik Faessler, Sascha Schäuble, Udo Hahn, Kathrin Thedieck, Gerald Radziwill, and Bettina Warscheid*

Cite This: https://doi.org/10.1021/acs.jproteome.2c00505 Read Online

ACCESS | Metrics & More | Article Recommendations | Supporting Information

ABSTRACT: Phosphorylation-dependent signal transduction plays an important role in regulating the functions and fate of skeletal muscle cells. Central players in the phospho-signaling network are the protein kinases AKT, S6K, and RSK as part of the PI3K-AKT-mTOR-S6K and RAF-MEK-ERK-RSK pathways. However, despite their functional importance, knowledge about their specific targets is incomplete because these kinases share the same basophilic substrate motif RxRxxp[ST]. To address this, we performed a multifaceted quantitative phosphoproteomics study of skeletal myotubes following kinase inhibition. Our data corroborate a cross talk between AKT and RAF, a negative feedback loop of RSK on ERK, and a putative connection between RSK and PI3K signaling. Altogether, we report a kinase target landscape containing 49 so far unknown target sites. AKT, S6K, and RSK phosphorylate numerous proteins involved in muscle development, integrity, and functions, and signaling converges on factors that are central for the skeletal muscle cytoskeleton. Whereas AKT controls insulin signaling and impinges on GTPase signaling, nuclear signaling is characteristic for RSK. Our data further support a role of RSK in glucose metabolism. Shared targets have functions in RNA maturation, stability, and translation, which suggests that these basophilic kinases establish an intricate signaling network to orchestrate and regulate processes involved in translation.

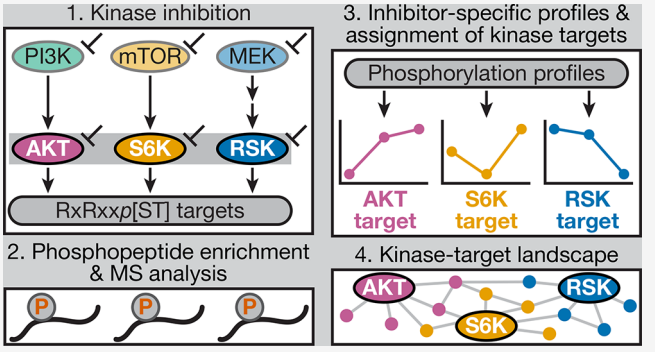

KEYWORDS: *skeletal muscle cells, signal transduction, kinase inhibitors, cross talk, kinase−substrate relationship, RXRXXS/T motif, protein phosphorylation, mass spectrometry, quantification, stable isotope labeling by amino acids in cell culture, label-free, parallel reaction monitoring (PRM), kinase−substrate enrichment analysis (KSEA), text mining*

INTRODUCTION

The phosphoinositide 3-kinase (PI3K)−AKT−mechanistic target of rapamycin (mTOR)−70 kDa ribosomal protein S6 kinase (S6K) and RAF−mitogen-activated protein kinase kinase (MEK)−extracellular signal-regulated kinase (ERK)−90 kDa ribosomal protein S6 kinase (RSK) signaling pathways regulate important physiological processes in skeletal muscle, which include myoblast proliferation and differentiation into myocytes during myogenesis,[1−5] glucose homeostasis,[6] hypertrophy,[7−10] and fiber-type determination[11−13] in mature myotubes. The Ser/Thr kinases AKT, S6K, and RSK are central members of this signaling network. All three kinases belong to the "AGC" kinase family, which are activated by a common mechanism that involves phosphorylation within the conserved activation loop and the C-terminal hydrophobic motif by 3-phosphoinositide-dependent protein kinase (PDK) 1 and a PDK2, respectively.[14−16] Notably, they share the basophilic substrate recognition motif RxRxxp[ST],[17] which poses a major challenge to the identification of their specific substrates.[18]

AKT is activated downstream of growth factor receptors, such as the insulin-like growth factor 1 (IGF-1) receptor. In this process, AKT is recruited to the plasma membrane by PI3K to become phosphorylated at T308 by PDK1.[10,19] Phosphorylation of S473 by a PDK2, such as the mechanistic target of rapamycin complex (mTORC) 2, further elevates AKT activity.[20−22] AKT phosphorylates numerous substrates to control physiological responses. For example, AKT promotes cell survival and glycogen synthesis by inhibitory phosphorylation of Bcl2-associated agonist of cell death (BAD)[23] and glycogen synthase kinase-3 (GSK-3),[24,25] respectively. To enhance cell growth,

Received: August 20, 2022

AKT activates mTORC1 *via* inhibitory phosphorylation of the negative regulators TSC complex subunit 2 (TSC2) and AKT1 substrate 1 (AKT1S1).[26,27]

S6K is an important effector downstream of mTORC1. It is activated by phosphorylation at T389 by mTORC1 and at T229 by PDK1.[28,29] S6K promotes protein synthesis by phosphorylation of the eukaryotic initiation factor 4B (eIF-4B), eukaryotic elongation factor 2 kinase (eEF2K), and 40S ribosomal protein S6 (RPS6), with the latter of those playing a role in ribosome biogenesis.[30−33]

RSK is a central effector of the mitogen-activated protein kinase (MAPK) signaling pathway. MAPK signaling cascades link extracellular signals to fundamental cellular processes including proliferation, differentiation, survival, and apoptosis.[34] Signaling downstream of growth factor receptors involves the activation of the proline-directed kinases ERK1/2 by the MAPK module, which comprises RAF and MEK1/2. ERK forms a complex with RSK and induces a multistep activation mechanism of RSK.[35] RSK promotes cell survival by phosphorylating BAD and is also involved in protein synthesis, as it shares the S6K targets RPS6 and eEF2K.[33,36,37] While knowledge about the multiple functions of the RAF-MEK-ERK cascade in contracting skeletal myotubes is still incomplete, recent studies suggest that it promotes the fast-twitch muscle fiber type.[11−13]

The PI3K-AKT-mTORC1-S6K and RAF-MEK-ERK-RSK pathways are interconnected and fine-tuned by several feedback loops and cross talk mechanisms. For example, the S6K-mediated phosphorylation of the insulin receptor substrate (IRS) 1 and the mTORC2 scaffold protein RPTOR independent companion of MTOR complex 2 (RICTOR) negatively regulates AKT.[38−40] RSK impinges on mTORC1 by inhibitory phosphorylation of TSC2.[26] In skeletal myotubes, both pathways are connected through the AKT-mediated inhibition of the RAF-MEK-ERK-RSK pathway, potentially by phosphorylation of RAF.[41−44] The high network interconnectivity poses a challenge for the accurate assignment of substrates to the three basophilic kinases AKT, S6K, and RSK.

We performed quantitative phosphoproteomics analyses to pinpoint phosphorylation targets of AKT, S6K, and RSK in fully differentiated, contracting skeletal myotubes. For this, we modulated the PI3K-AKT-mTOR-S6K and RAF-MEK-ERK-RSK pathways using kinase-specific inhibitors and pathway activators, followed by phosphoproteome profiling. Through bioinformatics analysis and data integration, we obtained kinase-specific candidates that were further assessed using targeted phosphoproteomics. Based on our data, we established an AKT, S6K, and RSK phosphorylation target landscape containing 49 so far unknown target sites. We show that each basophilic kinase targets a specific set of proteins with central roles in muscle development, integrity, and functions, as well as cytoskeletal organization. Furthermore, AKT is strongly associated with insulin and GTPase signaling and RSK with nuclear processes. Phosphorylation targets with functions in RNA metabolism are shared between AKT and S6K or RSK, which points to intricate regulatory mechanisms involved in RNA-dependent processes including translation.

EXPERIMENTAL SECTION

Cell Culture

C2 myoblasts (kind gift of D. Fürst, University of Bonn, Germany) were cultured in Dulbecco's modified Eagle's medium (DMEM) GlutaMAX (Gibco) supplemented with 15% (v/v) fetal calf serum (FCS, Anprotec), 2 mM sodium pyruvate (Life Technologies), and 1% (v/v) non-essential amino acids (NEAA, Life Technologies). Differentiation was induced by serum reduction to 2% (v/v) horse serum (Sigma-Aldrich) at 90−95% confluency. For stable isotope labeling by amino acids in cell culture (SILAC)[45]-based experiments, C2 mouse myoblasts were cultured in high-glucose SILAC−DMEM lacking arginine and lysine (PAA, GE Healthcare Life Sciences) supplemented with 15% (v/v) dialyzed FCS (Sigma-Aldrich), 2 mM sodium pyruvate, 1% (v/v) NEAA, 2 mM glutamine, 200 mg/L proline (all Thermo Fisher Scientific), 146 mg/L lysine, and 84 mg/L arginine (Cambridge Isotope Laboratories Inc.) for at least nine cell divisions. Light labeling was performed using $^{12}C_6{}^{14}N_4$−L-arginine/$^{12}C_6{}^{14}N_4$−L-lysine. For medium-heavy and heavy labeling, $^{13}C_6{}^{14}N_4$−L-arginine/D_4−L-lysine and $^{13}C_6{}^{15}N_4$−L-arginine/$^{13}C_6{}^{15}N_2$−L-lysine were used, respectively. Incorporation of labeled amino acids into the proteome was confirmed by liquid chromatography (LC)−mass spectrometry (MS) analysis. Labeled myoblasts were grown to confluency in six-well plates, and differentiation was induced by reducing the serum content to 2% (v/v) in-house dialyzed horse serum (Sigma-Aldrich) in the absence of sodium pyruvate.

For global quantitative phosphoproteomics profiling of AKT, S6K, and RSK kinase−substrate relationships, SILAC-labeled myotubes were serum-starved overnight and treated with electrical pulse stimulation (EPS; 10 V, 4 ms, 0.05 Hz) for 3 h using a C-Pace EP cell culture stimulator (IonOptix LLC) to obtain contracting myotubes.[46,47] During the last hour of EPS, cells were treated with 10 μM MK-2206 (MK; Selleck Chemicals, #S1078), 10 μM U0126 (U0; Selleck Chemicals, #S1102), 10 μM LY294002 (LY; Selleck Chemicals, #S1105), and 10 nM Torin1 (To; Merck, #475991) or dimethyl sulfoxide (DMSO; Sigma-Aldrich, #D8418).

For phosphoproteomics using direct kinase inhibition, a label-free global and a targeted MS approach were applied, in the following referred to as "label-free experiment" and "targeted MS experiment", respectively. Differentiated C2 myotubes were serum-starved for 4 h and treated with EPS for 3 h. Prior to lysis, cells were stimulated with IGF-1 (IGF; 10 ng/mL, Merck, #I1271) for 30 min or the epidermal growth factor (EGF; 10 ng/mL, Sigma-Aldrich, #E9644) for 15 min. MK (10 μM, 30 min), PF-4708671 (PF; 10 μM, Merck, #559273, 30 min), and BI-D1870 (BI; 10 μM, Selleck Chemicals, #S2843, 15 min) were used for kinase inhibition. Control cells were treated with a stimulator and DMSO (Roth, #A994).

As this study was performed using a murine cell line, phosphosite positions refer to the mouse annotation. For *bona fide* targets, the human phosphosite position is mentioned in brackets, if it differs from the mouse annotation.

Cell Lysis

SILAC-labeled cells were washed twice with ice-cold DPBS containing 0.75 mM $CaCl_2$ and 0.75 mM $MgCl_2$. Subsequently, cells were lysed using either urea buffer (30 mM Tris pH 8.5, 7 M urea, 2 M thiourea) for MS-based analysis or modified radioimmunoprecipitation assay (RIPA) buffer (150 mM NaCl, 1% [v/v] Nonidet-P40, 50 mM Tris pH 7.4, 0.25% [w/v] sodium deoxycholate) for immunoblotting. Both urea and modified RIPA buffer were supplemented with phosphatase inhibitors (2 mM sodium orthovanadate, 9.5 mM sodium fluoride, 10 mM β-glycerophosphate, 10 mM sodium

https://doi.org/10.1021/acs.jproteome.2c00505
J. Proteome Res. XXXX, XXX, XXX−XXX

pyrophosphate). Following sonication for 2 × 30 s, the lysates were cleared by centrifugation for 20 min at 4 °C and 21,100*g*.

Cells used in label-free and targeted MS experiments were lysed according to the EasyPhos protocol using 4% [w/v] sodium deoxycholate in 100 mM Tris-buffer, pH 8.5.[48] Protein concentrations of cleared lysates were determined using the Bradford assay (Bradford Quickstart reagent, Bio-Rad).

Gel Electrophoresis and Immunoblotting

Lysates were mixed with Lämmli buffer (2% [w/v] sodium dodecyl sulfate [SDS], 10% [v/v] glycerol, 0.25 M Tris HCl, pH 6.8, 5% [v/v] β-mercaptoethanol, bromphenol blue) and incubated for 10 min at 95 °C. Myotube lysates were separated on BisTris gradient gels (Thermo Fisher Scientific) or SDS polyacrylamide gels. Electrophoresis was conducted for 20 min at 80 V, followed by 1.5 h at 130 V using 3-(*N*-morpholino)-propanesulfonic acid (MOPS) (50 mM MOPS, 50 mM Tris base, 1% [w/v] SDS, 1 mM ethylenediaminetetraacetic acid [EDTA]) or SDS (25 mM Tris base, 200 mM glycine, 0.1% [w/v] SDS) running buffer for BisTris and SDS gels, respectively. Afterward, proteins were transferred to poly(vinylidene difluoride) membranes using either a tank or semidry blotting system. Tank blotting was conducted for 95−110 min at 45 V using 10% (v/v) methanol, 50 mM Tris, 100 mM glycine, and 0.01% (w/v) SDS (pH 8.3). Semidry blotting was performed at 0.22 A per membrane for 60 min using 20% (v/v) methanol, 48 mM Tris, 39 mM glycine, and 1.3 mM SDS (pH 9.1). Afterward, membranes were blocked with 5% (w/v) bovine serum albumin in Tris-buffered saline supplemented with Tween-20 (165 mM sodium chloride, 50 mM Tris HCl pH 7.4, 0.1% [v/v] Tween-20). Membranes were cut into smaller pieces to probe the membrane with different primary antibodies in parallel. Incubation of membrane pieces with primary and horseradish peroxidase-coupled secondary antibodies was performed overnight at 4−10 °C or for 2 h at room temperature (RT). Information about antibodies used is provided in the Supporting Information, Supplemental Experimental Table 1. Chemiluminescence signals were detected using a ChemoCam (INTAS) or a LAS-4000 minicamera system (GE Healthcare). For quantification of immunoblot signals, raw images were inverted, signal intensities per area were analyzed, and background intensities were subtracted using the software Quantity One (Bio-Rad, version 4.6.6). Signal intensities were normalized to the control, and mean phospho-to-total signal ratios were statistically characterized by the standard error of the mean and a Student's *t*-test (two-tailed, paired).

Protein Digestion and Desalting of Peptides

Cell lysates of SILAC-based experiments were mixed in equal amounts according to protein concentrations. For each experiment, a total of 3 mg of protein were used. Cysteine residues were reduced with 5 mM tris(2-carboxyethyl)-phosphine (20 min at RT) and alkylated using 50 mM 2-chloroacetamide (20 min at 37 °C). The reaction was quenched by the addition of 10 mM dithiothreitol. Samples were diluted with 50 mM ammonium bicarbonate to a final concentration of 2 M urea. Protein digestion using trypsin (Promega Corporation; trypsin/protein ratio of 1:50 [w/w]) was performed for 3.5 h at 42 °C and 500 rpm. The reaction was quenched by addition of 1% (v/v) final concentration of trifluoroacetic acid (TFA). The resulting peptide samples were desalted using Oasis HLB cartridges (Waters Corporation). Cartridges were conditioned using 4 mL of elution buffer (5% [v/v] formic acid [FA], 90% [v/v] acetonitrile [ACN]), and 4 mL of washing buffer (0.1% [v/v] TFA). After sample loading, cartridges were washed with 3 mL of washing buffer and 2 mL of ultrapure water. Peptides were eluted using 2 mL of elution buffer. Eluates were concentrated in a vacuum centrifuge for 30 min and lyophilized overnight and stored at −80 °C.

For label-free phosphoproteomics and targeted MS analyses, lysates containing 530 μg of protein were processed according to the EasyPhos workflow.[48] In brief, cysteine residues were reduced and alkylated with 10 mM tris(2-carboxyethyl)-phosphine and 40 mM 2-chloroacetamide for 5 min at 45 °C. Subsequently, protein digestion was performed in lysis buffer overnight at 37 °C using a combination of trypsin and LysC (FUJIFILM Wako Chemicals Europe GmbH; both protease/protein ratio 1:100 [w/w]).

Peptide Fractionation

Lyophilized peptides of SILAC myotubes were resolved in 200 μL of solvent A (10 mM ammonium hydroxide, pH 10), sonicated for 3 min, cleared for 4 min at 21,100*g*, and filtered using a 0.2 μm syringe filter (Phenomenex). High pH reversed-phase (hpH RP) chromatography was performed on a Dionex Ultimate 3000 equipped with an RP Gemini C18 column (4.6 mm × 25 mm, 3 μm, 110 Å, Phenomenex) operated at 750 μL/min. Peptides were loaded at 1% solvent B (10 mM ammonium hydroxide in 90% [v/v] ACN, pH 10) for 5 min and subsequently separated applying a gradient ranging from 1 to 20% B in 35 min, 20 to 45% B in 20 min, 11 min at 78% B, and 78 to 1% B in 10 min, followed by re-equilibration of the column at 1% B. Ninety fractions were collected in 50 s intervals between 2 and 77 min in a way that each 30th fraction was pooled. Samples were acidified with 1% (v/v) final concentration of TFA. From each fraction, a small aliquot of 20 μL was taken, dried *in vacuo*, and used for total proteome analysis, whereas the remaining part of the fractions was used for phosphoproteomics analysis.

Phosphopeptide Enrichment

Phosphopeptides of the SILAC-based experiments were enriched from fractionated samples in a batch procedure using 25 μL of titanium dioxide (TiO_2) bead slurry (bead/ACN ratio of 1:2 [v/v]; Titansphere, 5 μm, GL Sciences Inc.). After two washing steps with 200 μL of washing buffer (80% [v/v] ACN, 0.1% [v/v] TFA), 100 μL of 1× loading buffer (20% [v/v] acetic acid, 20 mg/mL 2,5-dihydroxybenzoic acid, 420 mM 1-octanesulfonic acid, 0.1% [v/v] heptafluorobutyric acid) was added to the beads. Each sample was mixed 1:1 with 2× loading buffer and incubated with TiO_2 beads for 20 min at 10 °C on a tube rotator. Subsequently, the beads were pelleted (5 min at 4 °C and 4696*g*), washed with 2 × 200 μL washing buffer, and incubated with 50 μL of elution buffer (50 mM ammonium dihydrogenphosphate, pH 10.5) for 10 min while rotating. Afterward, each sample was mixed in a ratio of 1:1 with ACN (v/v) and transferred to a StageTip comprising three layers of C8 material (3M Company). After centrifugation for 3 min at 1500*g*, phosphopeptide-enriched eluates were acidified using 8 μL of 100% TFA, dried *in vacuo*, and stored at −80 °C until used for LC-MS analysis.

Phosphopeptides of label-free and targeted MS experiments were enriched according to the EasyPhos workflow using TiO_2.[48] Phosphopeptides that still remained in the supernatants of the TiO_2-based enrichment step were subsequently enriched following the sequential metal oxide affinity chromatography (SMOAC) protocol.[49] For this purpose, 100 μL of 5% Fe(III)-immobilized metal affinity chromatography (IMAC) bead slurry (v/v) per sample was prepared from Ni^{2+}-nitrilotriacetic acid

https://doi.org/10.1021/acs.jproteome.2c00505
J. Proteome Res. XXXX, XXX, XXX−XXX

magnetic beads (Qiagen) and used as described before.[47] Eluates from TiO_2- and Fe(III)-IMAC-based enrichments were desalted using C18 StageTips (3M Company), pooled, and stored at −80 °C until used for LC-MS analysis. One half of the enriched samples was used for the label-free and targeted MS experiments.

LC-MS Analysis

Dried peptides were resolved in 0.1% (v/v) TFA and analyzed by nano-LC-MS/MS using a Velos Orbitrap Elite Pro (*i.e.*, for total proteome and the first technical replicate of the phosphoproteome analysis of SILAC experiments) or a Q Exactive Plus instrument (second technical replicate of the SILAC phosphoproteome analysis, label-free and targeted MS experiments) (Thermo Fisher Scientific, Bremen, Germany), both connected to an UltiMate 3000 RSLCnano HPLC system (Thermo Fisher Scientific, Dreieich, Germany). The RSLC systems were either equipped with PepMap C18 μ-precolumns (5 mm × 0.3 mm; particle size, 5 μm; packing density, 100 Å; Thermo Fisher Scientific) and an Acclaim PepMap C18 analytical column (500 mm × 0.75 mm; particle size, 2 μm; packing density, 100 Å; flow rate, 0.25 μL/min; Thermo Fisher Scientific) for the analysis of all samples obtained in SILAC experiments or with μPAC C18 precolumns (PharmaFluidics) and a μPAC C18 analytical column (length, 50 cm; flow rate, 0.3 μL/min; PharmaFluidics) for samples of label-free and targeted MS experiments. Peptide separation and elution were generally performed at 40 °C using a binary solvent system composed of 0.1% (v/v) FA/4% (v/v) DMSO (solvent A) and 50% (v/v) methanol/30% (v/v) ACN/0.1% (v/v) FA/4% (v/v) DMSO (solvent B) for measurements on the Orbitrap Elite or 0.1% (v/v) FA (solvent A′) and 86% (v/v) ACN/0.1% (v/v) FA (solvent B′) for analyses on the Q Exactive.

For measurements on the Orbitrap Elite, peptides were loaded at 1% B for 15 min and eluted with a gradient ranging from 1 to 40% B in 60 min, 40 to 65% B in 35 min, 65 to 99% B in 5 min, and 5 min at 99% B. The same gradient was applied for the analysis of the second technical replicate of the SILAC-based phosphoproteome analysis at the Q Exactive using the A′/B′ solvent system. Peptide mixtures of label-free and targeted MS experiments were loaded at 1% B′ for 3 min, followed by 1−3% B′ in 0.5 min, 3−22% B′ in 141.5 min, 22−39% B′ in 57 min, 39−54% B′ in 10 min, 54−95% B′ in 3 min, and 4 min at 95% B′ for peptide elution.

Acquisition of mass spectrometric data on the Orbitrap Elite was performed using the following parameters: MS scans, m/z 370−1700; resolution, 60,000 (at m/z 400); automatic gain control, 10^6 ions; max. ion time (IT), 200 ms. Samples of total proteome analyses were analyzed following a TOP20 method for fragmentation of multiply charged peptide ions by collision-induced dissociation applying an activation q of 0.25, an activation time of 30 ms, a normalized collision energy of 35%, an automatic gain control of 5×10^3, a max. IT of 150 ms, and a dynamic exclusion time of 45 s. For SILAC-based phosphoproteome analysis (first technical replicate), a TOP15 method was applied using multistage activation for peptide fragmentation considering precursors with neutral loss masses of 32.67, 49.00, or 98.00 Da; an automatic gain control of 10^4; and a max. IT of 100 ms. Parameters for mass spectrometric measurements on the Q Exactive were as follows: MS scans, 375−1700 m/z; resolution, 70,000 (at m/z 200); automatic gain control, 3×10^6; max. IT, 50 ms for targeted MS experiments and 60 ms for label-free and the second technical replicate of the SILAC-based phosphoproteome analysis. Multiply charged peptide ions were fragmented by higher-energy collisional dissociation applying a normalized collision energy of 28% and a dynamic exclusion time of 45 s. A TOP15 method was applied to analyze peptides of the second technical replicate of the SILAC-based phosphoproteome and label-free experiments at a resolution of 35,000, an automatic gain control of 10^5, and a max. IT of 120 ms. For targeted MS experiments, the resolution was set to 17,500, the automatic gain control to 2×10^5, and the max. IT to 50 ms.

To analyze samples of targeted MS experiments by parallel reaction monitoring (PRM), an inclusion list was generated using the software Skyline daily (version 20.2.1.384).[50] This list contained m/z values and retention time information of 11 iRT standard peptides (Biognosys), 16 internal control phosphopeptides, and 391 phosphopeptides (506 precursor ions) containing the RxRxx*p*[ST] motif, which were identified in our SILAC and label-free experiments. For inclusion in this list, RxRxx*p*[ST]-containing phosphopeptides of the SILAC-based experiment were filtered for a $\log_2$ fold change (FC) of <−0.3 and an adjusted p-value of <0.05. These peptides were matched to the global label-free dataset for retention time information. RxRxx*p*[ST]-containing phosphopeptides of the label-free experiment were required to have a $\log_2$ FC of <0 and to include an adjusted p-value of <0.1. The internal control phosphopeptides were selected based on the results of the label-free global screen ($\log_2$ FC < 1.125, adjusted p-value >0.5).

Database Searches and Peptide Spectrum Analysis

Rawfiles were analyzed using MaxQuant software (version 1.5.2.8 for SILAC experiments, version 1.6.10.43 for label-free and targeted MS experiments) equipped with the Andromeda search engine.[51,52] For database search, an *in silico* tryptic digest of a *Mus musculus* proteome from the UniProt sequence database was used (SILAC experiments: downloaded March 2015, containing 53,213 entries; label-free and targeted MS experiments: June 2020, 63,722 entries).

MaxQuant data processing was performed using the following parameters: variable modifications, S/T/Y phosphorylation, M oxidation, and N-term acetylation; fixed modification, C carbamidomethylation; first search mass tolerance, 20 ppm; false discovery rate (FDR), 1%; precursor ion mass tolerance, 4.5 ppm; fragment ion mass tolerance, 20 ppm (Q Exactive) or 0.5 Da (Orbitrap Elite); enzyme, trypsin/P; peptide charge states, +1 to +7; and "match between runs", enabled. For SILAC experiments, the following additional parameters were selected: max. missed cleavages, three; min. unique peptides, one; max. modifications per peptide, seven; matching time window, 5 min; "requantify", enabled; multiplicity of labeling states, three; and Lys-0/Arg-0, Lys-4/Arg-6, and Lys-8/Arg-10 were set as light, medium-heavy, and heavy labels, respectively. For label-free/targeted MS experiments, the following additional parameters were selected: max. missed cleavages, two/three; min. unique peptides, one/none; max. modifications per peptide, five; and matching time window, 0.7 min. Due to an unstable electrospray, MS data for IGF replicate 1 and BI replicate 3 were not considered in further analyses. Reverse, potential contaminant, and "only identified by site" hits were removed, and mean $\log_2$ ratios were calculated (experiment *vs* control). For the identified isoforms of AKT, S6K, and RSK, intensity-based absolute quantification (iBAQ) values[53] were calculated based on the protein group mean intensities.

https://doi.org/10.1021/acs.jproteome.2c00505
J. Proteome Res. XXXX, XXX, XXX−XXX

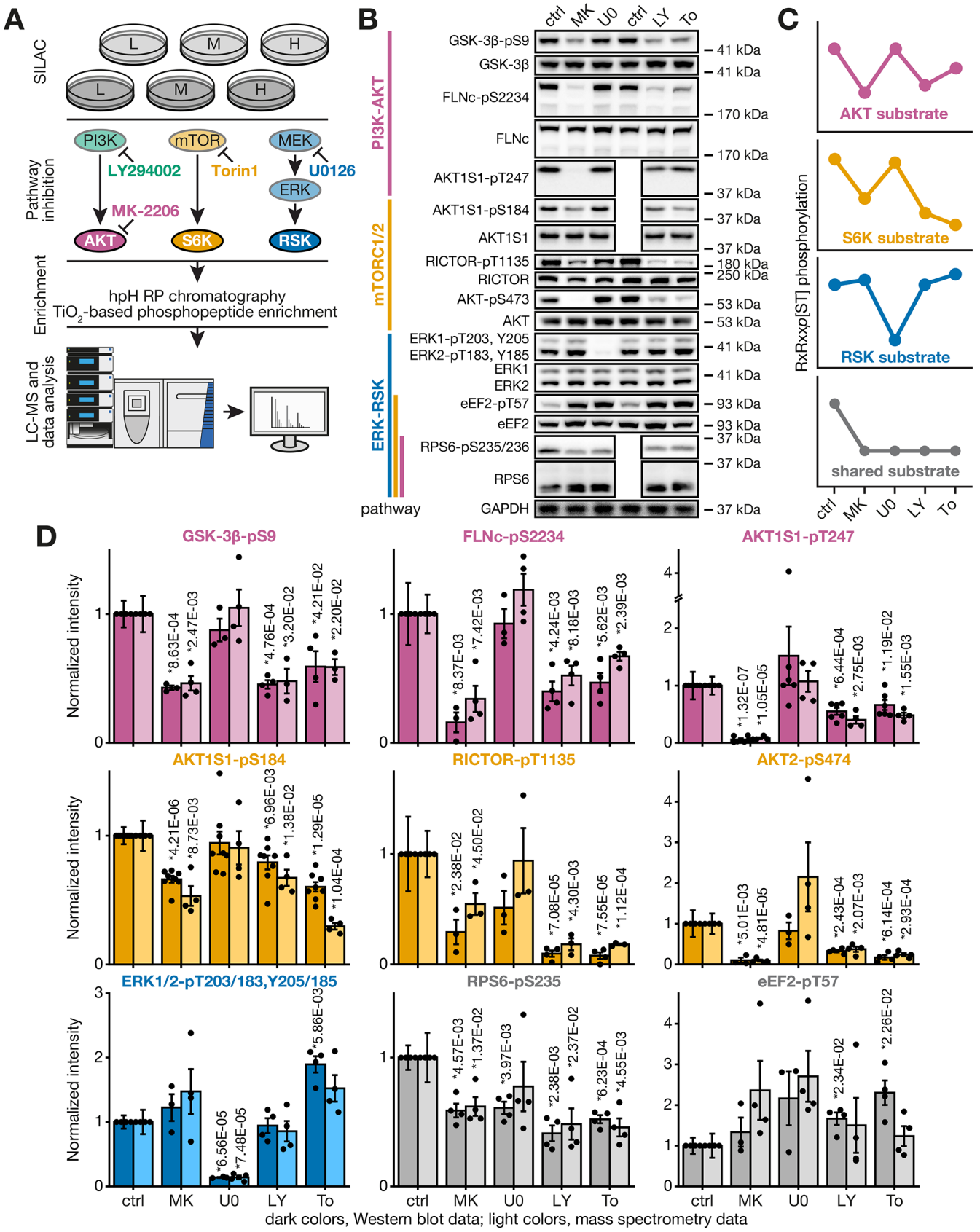

Figure 1. Phosphoproteomics profiling approach to study AKT, S6K, and RSK targets in skeletal myotubes. (A) SILAC-labeled contracting C2 myotubes were treated with 10 μM LY294002, 10 μM MK-2206, 10 nM Torin1, or 10 μM U0126 for 1 h. Control cells were treated with DMSO. To compare four different inhibitors, two triple SILAC experiments were combined, using the control condition as reference between the experiments (n = 4 each). For global quantitative phosphoproteomics, cell lysates were mixed in a 1:1:1 ratio based on protein concentrations. Tryptic digests were fractionated using high pH reversed-phase (hpH RP) chromatography and enriched for phosphopeptides using TiO_2, followed by LC-MS and

https://doi.org/10.1021/acs.jproteome.2c00505
J. Proteome Res. XXXX, XXX, XXX−XXX

Figure 1. continued

bioinformatics data analysis. L/M/H, light/medium-heavy/heavy SILAC label. (B) Western blot analysis of the PI3K-AKT-mTOR-S6K and RAF-MEK-ERK-RSK pathways using protein- and phospho-specific antibodies against established pathway members. Glyceraldehyde 3-phosphate dehydrogenase (GAPDH) served as a loading control. Uncut blots for AKT1S1 and RPS6 are shown in Figure S1C. ctrl, control; MK, MK-2206; U0, U0126; LY, LY294002; and To, Torin1. (C) Expected inhibition profiles for the phosphorylation targets of AKT, S6K, and RSK upon treatment with the indicated pathway inhibitors. (D) Comparison of the Western blot (dark colors) and normalized MS signal intensities (light colors) for established PI3K-AKT-mTOR-S6K and RAF-MEK-ERK-RSK pathway members. Measured intensities were normalized to the control, and a two-tailed paired Student's *t*-test was performed (control *vs* treatment). Numbers above bars indicate the *p*-value, and the error bars represent the standard error of the mean (n = 3−8).

To analyze data of the targeted MS experiments, the inclusion list, the MaxQuant results file msms.txt (filtered for the PRM raw files), all PRM raw files, and the fasta file of the UniProt ProteomeSet for mouse (June 2020) were imported into Skyline. Peptide settings were as follows: protease, trypsin/P; max. missed cleavages, two; time window, 5 min; peptide length, 8−25 amino acids; modifications, cysteine carbamidomethylation, methionine oxidation, and S/T/Y phosphorylation; max. variable modifications, three; and max. neutral loss, one. Default orbitrap transition settings were applied. Due to an unstable electrospray, MS data of the following experiments were not considered in our analysis: IGF replicate 9, MK replicate 4, and PF replicate 5. Peptides with low-quality, interfered MS1 and/or number of MS2 <4 were discarded manually. For phosphopeptides with multiple precursor ions, only the one with the highest intensity and highest number of peptide spectral matches was kept for further analysis. Extracted ion chromatograms for all peptides were manually inspected for correct peak picking, and peak integrations were adjusted if needed. Total MS1 areas were exported as a pivot table,[54] and intensities were normalized to the mean intensity of 10 internal control phosphopeptides.

Data Availability

The mass spectrometry proteomics data have been deposited to the ProteomeXchange Consortium (http://proteomecentral.proteomexchange.org) *via* the PRIDE[55] partner repository with the dataset identifiers PXD018667 (SILAC phosphoproteomics experiment), PXD029678 (label-free global phosphoproteomics experiment), and PXD029633 (Targeted MS experiment). Processed data of the PRM assay analyzed with Skyline[50] are available on the PanoramaWeb platform[56] *via* https://panoramaweb.org/wQ4FF0.url.

Bioinformatics Analyses

Statistics. For the SILAC and label-free data, a linear model within the Limma framework, using an empirical Bayes procedure to moderate the variances, was applied to estimate effects of the inhibitors.[57] In this model, labeling effects were included to adjust for labeling bias. For the targeted MS data, a linear model without intercept was used to estimate the effect of the inhibitors and activators used. The following comparisons were made: (1) IGF *vs* MK, (2) IGF *vs* PF, and (3) EGF *vs* BI. For all datasets, the FDR was calculated with the Benjamini−Hochberg step-up procedure. Phosphosites with an FDR < 0.1 were considered as regulated.

Motif-x Analysis. The ±7 residue sequence window around phosphorylated residues of significantly regulated phosphopeptides was used as input for the motif-x package implemented in R.[58,59] The minimum motif occurrence was set to 20, and a *p*-value cutoff of 10^{-6} was applied. The visualization of the overrepresented sequences was done in Python using the Logomaker package.[60]

Kinase−Substrate Enrichment Analysis (KSEA). For KSEA, phosphosites were annotated with their respective upstream kinase(s) using the PhosphoSitePlus (download 09.10.2020) kinase−substrate dataset.[61−63] The annotation was restricted to kinase−substrate interactions reported *in vivo* in a murine background. Further, kinase isoforms were grouped together and only kinases with at least five substrates in the data were considered for further analysis. A score for each kinase was calculated with the following equation based on a *z*-score transformation: $\frac{(\overline{s}-\overline{p})\sqrt{m}}{\sigma}$. Here, $\overline{s}$ represents the mean $\log_2$ FC of a kinase's substrates, $\overline{p}$ represents the $\log_2$ FC of all quantified phosphopeptides, m is the total number of quantified phosphopeptides attributed to the respective kinase, and σ denotes the standard deviation of the $\log_2$ FC of all phosphopeptides.

Principal Component Analysis (PCA). PCA was performed with the PCA class of the scikit-learn library in Python. Prior to the PCA of experimental conditions, batch effects introduced by the labeling were removed with limma's removeBatchEffect() function. For PCA on RxRxx*p*[ST] motif clusterings, known AKT, S6K, and RSK substrates were annotated according to PhosphoSitePlus (download 09.10.2020).[63]

Hierarchical Cluster Analysis. Phosphosites with an FDR < 0.1 and a $\log_2$ FC < 0 for one of the inhibitors were included in the hierarchical cluster analysis. Here, the Euclidean distance in combination with Ward's method was used to generate the linkage with the scipy linkage function.[64,65]

Mapping of Human Sites and Protein Network Analysis. The respective orthologous human protein for a respective mouse protein was predicted using BLASTP.[66] Mouse and human protein sequences (UniProt, download 06.2016)[67] were aligned using the Biopython pairwise2 module (parameters: PAM30, version 1.0.6; open, −6; extend, −6).[68] Human sites were mapped according to the mouse phosphosite positions in the alignment. Validated known and new kinase targets were subjected to protein network analysis using the STRING database (www.string-db.org; version 11.5).[69] Default parameters were applied, and the edge thickness represents confidence of the protein−protein interaction.

RESULTS AND DISCUSSION

Profiling of AKT, S6K, and RSK Pathways in Skeletal Myotubes

To globally profile phosphorylation targets of AKT, S6K, and RSK in skeletal muscle cells, we performed pharmacological interventions at different pathway levels. We used fully differentiated and electrical pulse-stimulated contracting C2 skeletal myotubes as an established cell culture-based model system for skeletal muscle fibers.[47] In these functional, contracting mouse myotubes (Figure S1A), the signaling

https://doi.org/10.1021/acs.jproteome.2c00505
J. Proteome Res. XXXX, XXX, XXX−XXX

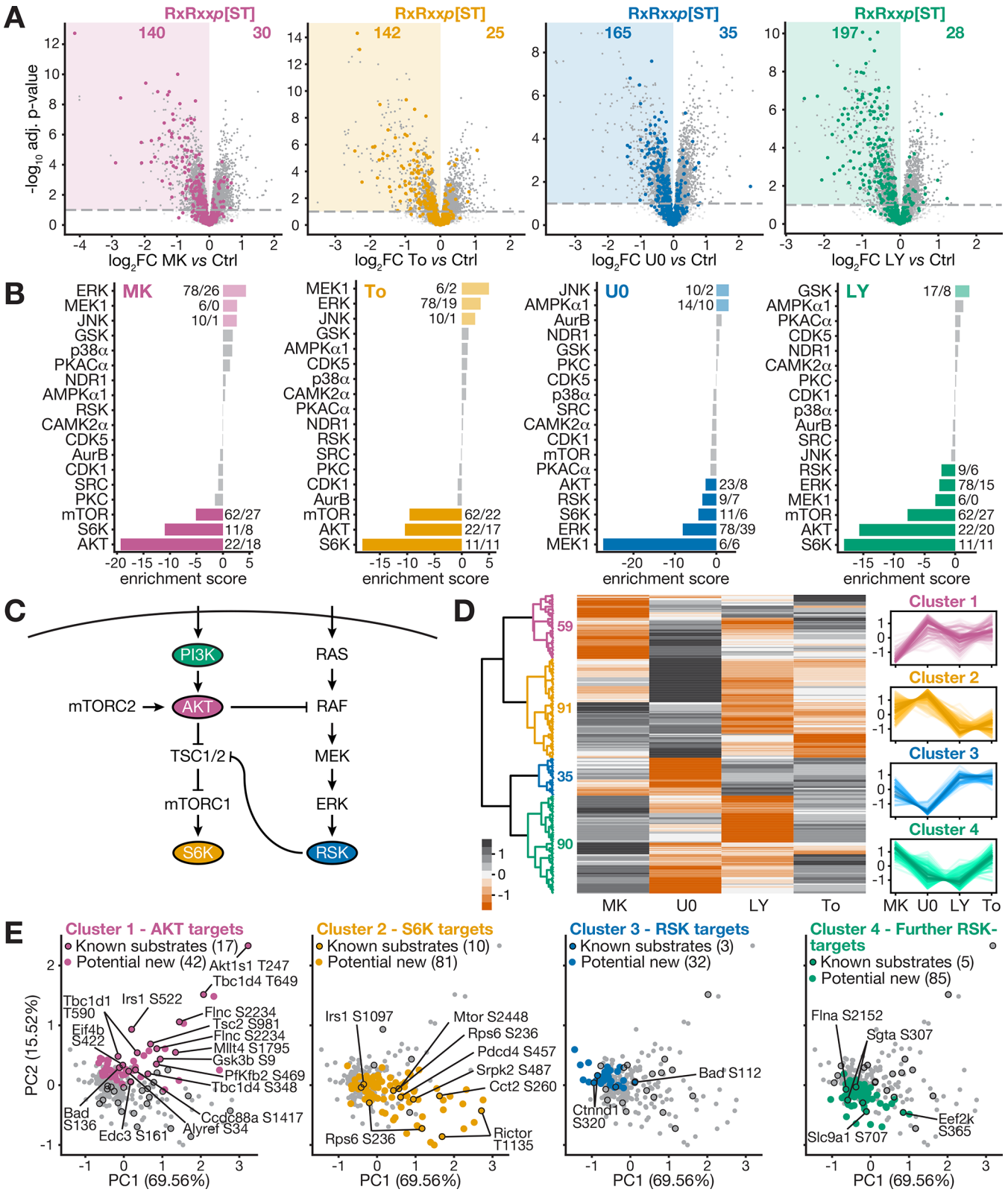

Figure 2. Phosphorylation within the basophilic motif RxRxx*p*[ST] is decreased upon PI3K-AKT-mTOR-S6K and RAF-MEK-ERK-RSK pathway inhibition. (A) Scatter plots of quantified phosphopeptides. Log_2-transformed fold change (FC; inhibitor treatment/control) was plotted against $-log_{10}$ values of adjusted *p*-values (two-tailed moderated Student's *t*-test). Phosphopeptides phosphorylated within the RxRxx*p*[ST] motif are highlighted. Dashed horizontal lines indicate an adjusted *p*-value of 0.1. (B) Results of kinase−substrate enrichment analyses based on log_2-transformed quantified phosphopeptide ratios (inhibitor treatment/control). Numbers indicate the number of quantified/significantly regulated substrates for significantly regulated kinases. (C) Overview of the PI3K-AKT-mTOR-S6K and RAF-MEK-ERK-RSK signaling interplay. (D) Hierarchical cluster analysis of the RxRxx*p*[ST]-containing phosphopeptides after *z*-score transformation. (E) Principal component analysis of the RxRxx*p*[ST]-containing phosphopeptides. Highlighted are known substrates and new targets identified in this analysis for each kinase. Annotations are according to entries in the PhosphoSitePlus database (*in vivo* and *in vitro* substrates in mouse).

https://doi.org/10.1021/acs.jproteome.2c00505
J. Proteome Res. XXXX, XXX, XXX−XXX

downstream of PI3K, AKT, mTOR, and MEK was blocked with the inhibitors LY294002 (LY), MK-2206 (MK), Torin1 (To), or U0126 (U0) (Figure 1A). Changes in protein phosphorylation were analyzed by quantitative phosphoproteomics using SILAC, TiO_2-based phosphopeptide enrichment of fractionated samples and LC-MS. The effectiveness of the kinase inhibitor treatments was confirmed by Western blot analysis using phospho-specific antibodies for established pathway readouts (Figures 1B and S1B,C). The inhibitors MK and LY inhibit AKT signaling by direct blockade or upstream inhibition, respectively (Figure 1A). MK and LY reduced phosphorylation of the AKT targets GSK-3β-S9,[25] filamin C (FLNc)-S2234 (human S2233),[70] and AKT1S1-T247 (human T246)[27] (Figure 1B). Since PI3K and AKT act upstream of mTORC1, their inhibition by LY and MK led to reduced phosphorylation of the mTORC1 target AKT1S1-S184 (human S183)[71] and, downstream of S6K, RICTOR-T1135.[40] We applied LY for inhibiting the PI3K-AKT-mTOR-S6K pathway, but LY can also directly affect mTOR activity.[72,73] Thus, to specifically inhibit the mTOR-S6K pathway, we employed To, which has been widely used for studying mTOR signaling.[74−77] Notably, we applied To at a concentration of 10 nM, which was shown to preclude off-target effects.[78] Following mTOR inhibition, we observed reduced phosphorylation of AKT substrates, although to a lesser extent. This is in line with previous work showing that mTOR acts on PI3K-AKT signaling by mTORC2-mediated phosphorylation of AKT-S473 (AKT1; AKT2, S474).[79−81] However, as To treatment also reduced AKT-T308 phosphorylation (Figure S1B), we cannot fully exclude a potential off-target effect on PI3K.[82] Targets of the MEK-ERK-RSK cascade (mouse: ERK1-T203/Y205, ERK2-T183/Y185; human: ERK1-T202/Y204, ERK2-T185/Y187) were not reduced by the inhibition of the PI3K-AKT-mTOR-S6K pathway (Figure 1B). Instead, ERK1/2 phosphorylation is slightly increased using MK and To, which is in accordance with the reported cross talk between AKT and RAF in myotubes.[41−44] In addition, there are also substrates which are shared targets of more than one pathway (Figure S1D and Supplemental Table 1).[33,37] Accordingly, phosphorylation of RPS6-S235/236 and eukaryotic elongation factor 2 (eEF2)-T57 were affected to similar extent by all inhibitors used here (Figures 1B and S1C).

Based on the Western blot data, we predicted generic inhibitor-dependent regulation profiles for phosphorylation targets of AKT, S6K, or RSK, as well as for shared substrates as illustrated in Figure 1C. We further anticipated that these phosphorylation profiles provide a valid approach to cope with the tight interconnection of the two signaling pathways and identify targets of AKT, S6K, and RSK, which share the basophilic motif RxRxx*p*[ST]. As a proof of concept, we generated quantitative Western blot and MS data of established pathway readouts (Figures 1D and S1E and Supplemental Table 1). The obtained site-specific data were highly consistent in terms of phospho-regulation of *bona fide* pathway members and confirmed the predicted kinase inhibitor-dependent regulation profiles (Figure 1C).

Pathway Inhibition Preferentially Targets the Basophilic Motif RxRxx*p*[ST]

Global quantitative phosphoproteomics analysis of cultured, contracting C2 myotubes as outlined in Figure 1A resulted in the identification of 8853 proteins, of which 4738 were phosphorylated on 33,964 sites (Figure S2A and Supplemental Table 2). A total of 21,611 phosphosites were localized with a probability >75%, with about 83.4% located on serine, 14.8% on threonine, and 1.8% on tyrosine residues (Figure S2A−D and Supplemental Table 2). The acquired MS data were consistent between treatments and biological replicates (n = 4), with 83.8% of the localized phosphosites quantified in at least two replicates (Figure S2E,F). The inhibitor treatments had no regulatory effect on the large majority of quantified phosphosites and the total proteome (Figure S2G,H). Quantitative analysis of the total proteome further showed the differences in the abundance of AKT, S6K, and RSK (Supplemental Table 2). We found that AKT2 was more abundant than AKT1, whereas AKT3 was hardly detected in C2 myotubes. This finding is in line with previous work showing that *Akt2* is highly expressed in insulin-sensitive tissues including skeletal muscle and adipocytes,[83−85] whereas *Akt1* is expressed in a wide range of tissues,[86,87] and *Akt3* has a more restricted tissue distribution with highest levels in the brain.[88,89] For S6K, we found isoform 1 to be more abundant than isoform 2. While both isoforms are ubiquitously expressed,[90,91] a role in muscle structure maintenance and force generation has been reported for S6K1.[92] Of the four RSK isoforms, we only detected RSK1 and RSK2 in C2 myotubes. Here, RSK2 is the major isoform, which has been shown to be highly expressed in skeletal muscle, heart, and pancreas.[35,93,94] For further C2 myotube phosphoproteome analysis, we considered 15,046 phosphopeptides (12,372 phosphosites), which were quantified in at least two replicates across conditions. PCA of the phosphopeptides showed that replicates of each inhibitor experiment cluster together (Figure S2I). In the first principal component (PC) 1, the U0 experiment separates from the other inhibitor treatments, whereas To separates from MK and LY treatments, in PC2, showing that the changes in phosphorylation are inhibitor-specific.

To globally analyze the specificity of the inhibitor treatments, we performed Motif-x analysis,[58,59] which confirmed the basophilic motif RxRxx*p*[ST] to be significantly enriched (p-value $<10^{-6}$) among the downregulated phosphopeptides for all treatments (Figures 2A and S3A and Supplemental Table 3). In addition, both the MAPK recognition motif Px*p*[ST]P and a short basophilic motif RR*p*[ST] were enriched upon MEK inhibition (Figure S3A−C). The latter motif has been described as a recognition motif for RSK and protein kinase A (PKA).[95−97] To test whether there is a connection between PKA and MEK-RSK signaling, contracting C2 myotubes were treated with EGF or Forskolin and IBMX (FI) to activate RSK and PKA or U0 or BI-D1870 (BI) to inhibit MEK and RSK, respectively (Figure S3D). However, we here show that phosphorylation levels of ERK1/2-pT203,Y205/T183,Y185, and the RSK substrate Catenin-δ-S320[98] are not affected by PKA activation and that the PKA substrate β-Catenin-S675 is not affected by EGF, U0, or BI treatment (Figure S3D). Furthermore, cluster analysis revealed that the RR*p*[ST] motif is most prominent for U0 treatment, whereas a comparably low number of peptides containing this motif are regulated upon AKT, PI3K, and mTOR inhibition (Figure S3E). Thus, our data corroborate RR*p*[ST] as an alternative recognition motif for RSK in C2 myotubes.[95]

Through kinase−substrate enrichment analysis (KSEA) and gene ontology (GO) term enrichment, we confirmed that the AKT pathway was mostly affected by MK and LY treatment (Figures 2B and S3F and Supplemental Table 3). Notably, LY can also directly affect mTOR, PIM1, DNAPK, and CK2.[72,73,99,100] Thus, an off-target effect of LY on mTOR might have contributed to the observed downregulation of mTOR substrates (Figure 2B). For PIM1, the substrate IRS2-

https://doi.org/10.1021/acs.jproteome.2c00505
J. Proteome Res. XXXX, XXX, XXX−XXX

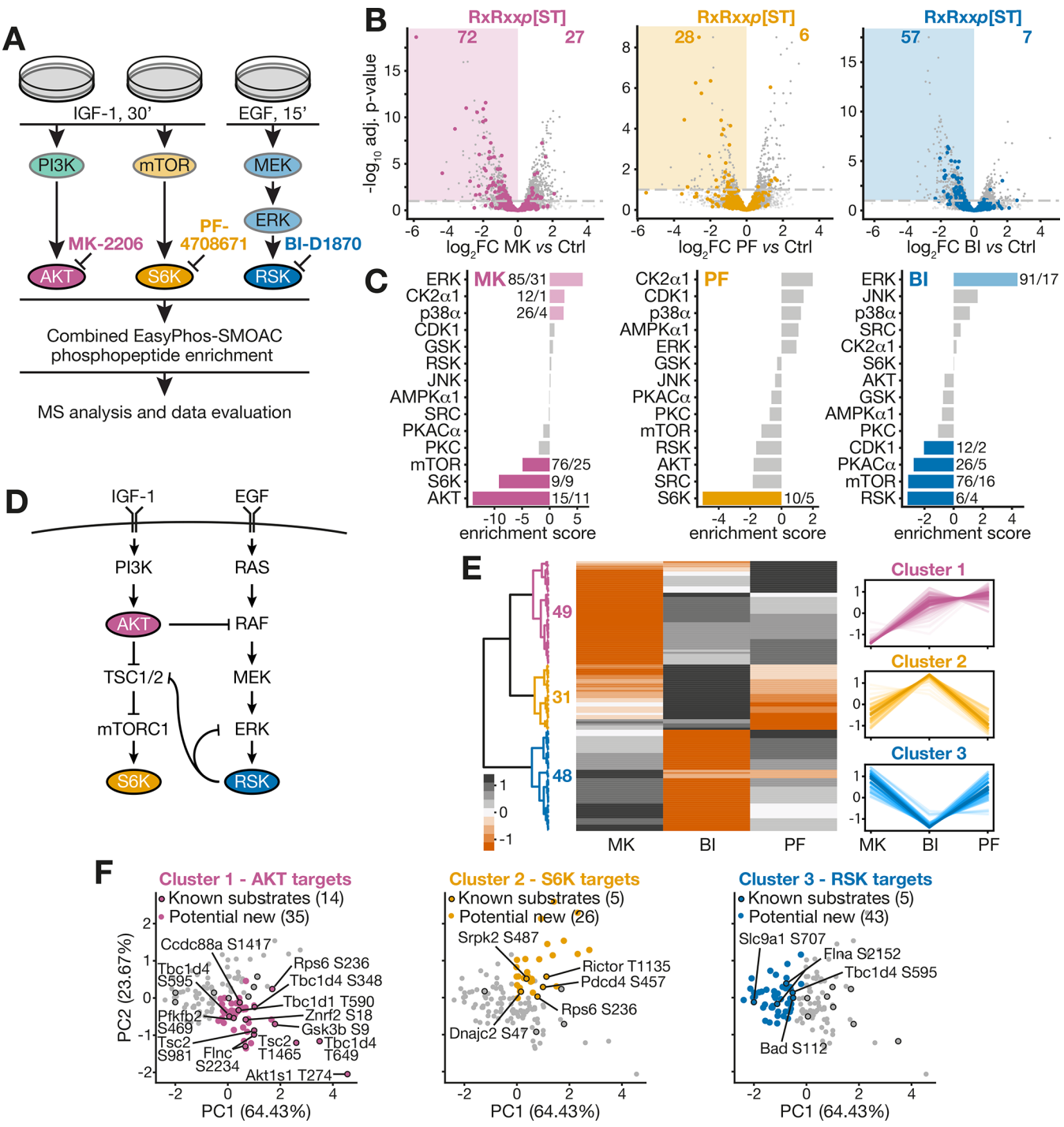

Figure 3. Label-free phosphoproteomics analysis of AKT, S6K, and RSK targets using combined pathway stimulation and kinase inhibition. (A) Contracting C2 myotubes were stimulated with IGF-1 (30 min, 10 ng/mL) or EGF (15 min, 10 ng/mL). Downstream signaling of AKT, S6K, and RSK was blocked using the specific inhibitors MK-2206 (30 min, 10 μM), PF-4708671 (30 min, 10 μM), and BI-D1870 (15 min, 10 μM), respectively. Phosphopeptides were sequentially enriched employing EasyPhos and SMOAC, followed by LC-MS and bioinformatics analysis. (B) Scatter plots of quantified phosphopeptides. Log_2-transformed fold changes (FC, fold change; inhibitor/stimulus) were plotted against $-\log_{10}$ values of adjusted *p*-values (two-tailed moderated Student's *t*-test). Phosphopeptides phosphorylated within the RxRxx*p*[ST] motif are highlighted. Dashed horizontal lines indicate an adjusted *p*-value of 0.1. MK, MK-2206; PF, 4708671; and BI, BI-D1870. (C) Results of kinase−substrate enrichment analyses based on log_2-transformed phosphopeptide ratios (inhibitor/stimulus). Numbers indicate the number of quantified/significantly regulated substrates for significantly regulated kinases. (D) Overview of the PI3K-AKT-mTOR-S6K and RAF-MEK-ERK-RSK signaling interplay. (E) Hierarchical cluster analysis and profile plots of the RxRxx*p*[ST]-containing phosphopeptides after *z*-score transformation. (F) Principal component analysis of the RxRxx*p*[ST]-containing phosphopeptides. Highlighted are known substrates and new targets for each kinase. Annotations are according to entries in the PhosphoSitePlus database (*in vivo* and *in vitro* substrates in mouse).

S1138 (human, S1149)[101] was slightly downregulated, whereas PSMD2-S361[102] was not regulated under LY treatment (Supplemental Table 2). Since the recognition motifs of CK2 ([ST][DE]x[DE])[103,104] and DNAPK ([ST]Q)[105] were also

https://doi.org/10.1021/acs.jproteome.2c00505
J. Proteome Res. XXXX, XXX, XXX−XXX

not enriched in the dataset (Supplemental Table 3), we concluded that LY had no effect on these kinases under the applied condition.

Reduced AKT activity upon To treatment can be attributed in part to reduced mTORC2-dependent AKT-S473 and PI3K-dependent AKT-T308 phosphorylation (Figures 2B,C and S3F, see also Figures 1B and S1B).[82] Off-target effects of To on DNAPK[78] and MEK have been reported (https://lincs.hms.harvard.edu/db/sm/10079-101/). However, the DNAPK recognition motif ([ST]Q)[105] was not enriched in our data (Supplemental Table 3), which is in line with previous work showing that To rather selectively inhibits mTOR in cellular assays when used at low concentrations (<1 μM).[78] Moreover, phosphorylated MEK1 and ERK substrates were enriched upon To treatment (Figure 2B), which confirms that To had also no off-target effect on MEK under the applied condition.[78]

Regulation of the mTOR-S6K pathway was prominent for To and LY and to a lesser extent for MK, whereas U0 treatment affected mostly MEK-ERK-RSK signaling (Figures 2B and S3F and Supplemental Table 3). The downregulation of S6K substrates upon MEK inhibition can be attributed to both, cross talk between RSK and TSC2[26] and shared substrates such as RPS6-S236[37] (Figure 2B,C; see also Figures 1B and S1D). Since KSEA showed an upregulation of MEK and ERK substrates upon MK and To treatment, our data corroborate the reported cross talk between AKT and the RAF-MEK-ERK-RSK pathway in skeletal myotubes[41−44] (Figure 2B,C). Interestingly, LY did not result in the upregulation of MEK and ERK substrates, but their downregulation. This finding is in line with other studies reporting a connection between PI3K and RAF-MEK-ERK.[106−108] However, further confirmation of this association is needed to exclude a potential off-target effect of LY on the RAF-MEK-ERK cascade.[109] Consistent with computational modeling data,[110] we observed slight upregulation of JNK substrates upon inhibition of AKT, mTOR, and MEK (Figure 2B and Supplemental Table 3).

AMP-activated kinase (AMPK) activation has been proposed to constitute an MAPK-independent off-target effect of U0.[111] Furthermore, U0 was shown to inhibit p38α, the p38-activated kinase PRAK, and AKT1 with a 5-fold lower potency than MEK.[99] In our analysis, neither p38 substrates nor the putative PRAK substrate PLA2G4A-S726 (human, S727)[112] was affected by U0 treatment (Figure 2B and Supplemental Table 2). Based on KSEA, a potential slight off-target effect of U0 on AKT substrates (Figure 2B) was indicated. However, this was not confirmed by quantitative analysis of the *bona fide* AKT substrates GSK-3β-S9, FLNc-S2234, and AKT1S1-T247 (Figure 1B,D). We next performed cluster analysis, which grouped RxRxx*p*[ST]-containing phosphopeptides into four distinct classes based on their kinase inhibitor-dependent regulation profiles (Figure 2D and Supplemental Table 4). The filtering for the basophilic motif served as an additional measure for selecting a valid set of regulated phosphopeptides for the identification of AKT, S6K, and RSK targets. The cluster tree suggests a strong relationship between AKT and S6K signaling and further indicates a potential connection between RSK- and PI3K-dependent signaling. These observations were supported by text mining of the clustering gene names in the published literature (Figure S3G and Supplemental Table 5). Text mining revealed that AKT is mostly associated with clusters 1 and 2, S6K with cluster 2, and RSK with cluster 4. Of note, cluster 3 does not show high enrichment for RSK due to a limited number of RSK-specific studies in the literature (Supplemental Table 5). In combination with PCA of the RxRxx*p*[ST] clusters and annotation of *bona fide* kinase substrates, we identified specific sets of new substrate candidates for AKT, S6K, and RSK (Figure 2E and Supplemental Table 4).

Direct Inhibition of AKT, S6K, and RSK for Phosphorylation Target Identification

To further pinpoint the specific targets of AKT, S6K, and RSK, we used a combination of pathway stimulation and direct kinase inhibition. PI3K-AKT-mTOR-S6K and RAF-MEK-ERK-RSK were activated using IGF-1 and EGF, whereas AKT, S6K, and RSK were simultaneously inhibited using MK, PF-4708671 (PF), and BI, respectively (Figure 3A). For quantitative phosphoproteomics, kinase activator and inhibitor treatments were optimized for C2 skeletal myotubes (Figures 3A and S4A−G). We assessed changes in the activity profiles of AKT, S6K, and RSK following MK, PF, and BI treatments (Figure S4D−G). As expected, MK treatment resulted in markedly reduced phosphorylation of AKT, S6K, and their *bona fide* substrates AKT1S1-T247 and GSK-3α/β-S21/S9 (for AKT) as well as RICTOR-T1135 and RPS6-S235/S236 (for S6K) (Figure S4D). Moreover, increased phosphorylation of RSK-S380 and the RSK substrate Catenin-δ-1-S320 upon MK treatment confirms the inhibitory cross talk between AKT and RAF-MEK-ERK signaling in myotubes.[41−44] PF has been previously used to inhibit S6K in myotubes.[113,114] Inhibition of S6K using PF markedly decreased phosphorylation of the S6K substrates RPS6-pS235/236 and RICTOR-T1135, without affecting the activity of AKT and RSK (Figure S4E,F). Following RSK inhibition using BI, AKT-T308 and S6K-T389 phosphorylation were reduced, whereas substrate phosphorylation (AKT1S1-T246 for AKT, RICTOR-T1135 for S6K, and RPS6-S235/236 for S6K/RSK) was virtually not affected, which is in particular true for the 15 min time point (Figure S4G). Thus, we concluded that the off-target effect of BI on AKT and S6K is minor and should not impede the identification of RSK targets through phosphoproteomics analysis. Phosphopeptides were enriched using the EasyPhos workflow, which enables efficient and robust quantitative phosphoproteomics in combination with label-free MS.[48] Moreover, with this streamlined workflow, we performed a second phosphopeptide enrichment step using SMOAC[49] and increased the number of biological replicates (n = 9) to better account for biological variation in signaling events. Data analysis resulted in the identification of 4077 phosphoproteins and 25,822 phosphosites (Figure S5A and Supplemental Table 6). The 17,379 localized phosphosites showed similar distributions of S/T/Y phosphorylation, phosphosites per peptide, and charge state as in the SILAC data (Figure S5B−D, see also Figure S2B−D). For each treatment set, more than 25,000 phosphopeptides were quantified, of which the large majority was not regulated (Figure S5A,E,F). In general, the correlation of data between biological replicates for different treatments was high (R 0.82−0.95) (Figure S5G).

As observed in the pathway profiling approach, direct kinase inhibition resulted in a prominent downregulation of the basophilic motif RxRxx*p*[ST] and known substrates of AKT, S6K, and RSK, including AKT1S1-T247, RICTOR-T1135, and BAD-S112, respectively (Figure 3B,C and Supplemental Table 7). In contrast to MK treatment, direct inhibition of the effector kinase S6K by PF did not affect the cross talk between AKT and the RAF-MEK-ERK-RSK pathway (Figure 3C,D). This is in line with previous work showing that the cross talk between AKT and the RAF-MEK-ERK-RSK pathway acts on the level of AKT

https://doi.org/10.1021/acs.jproteome.2c00505
J. Proteome Res. XXXX, XXX, XXX−XXX

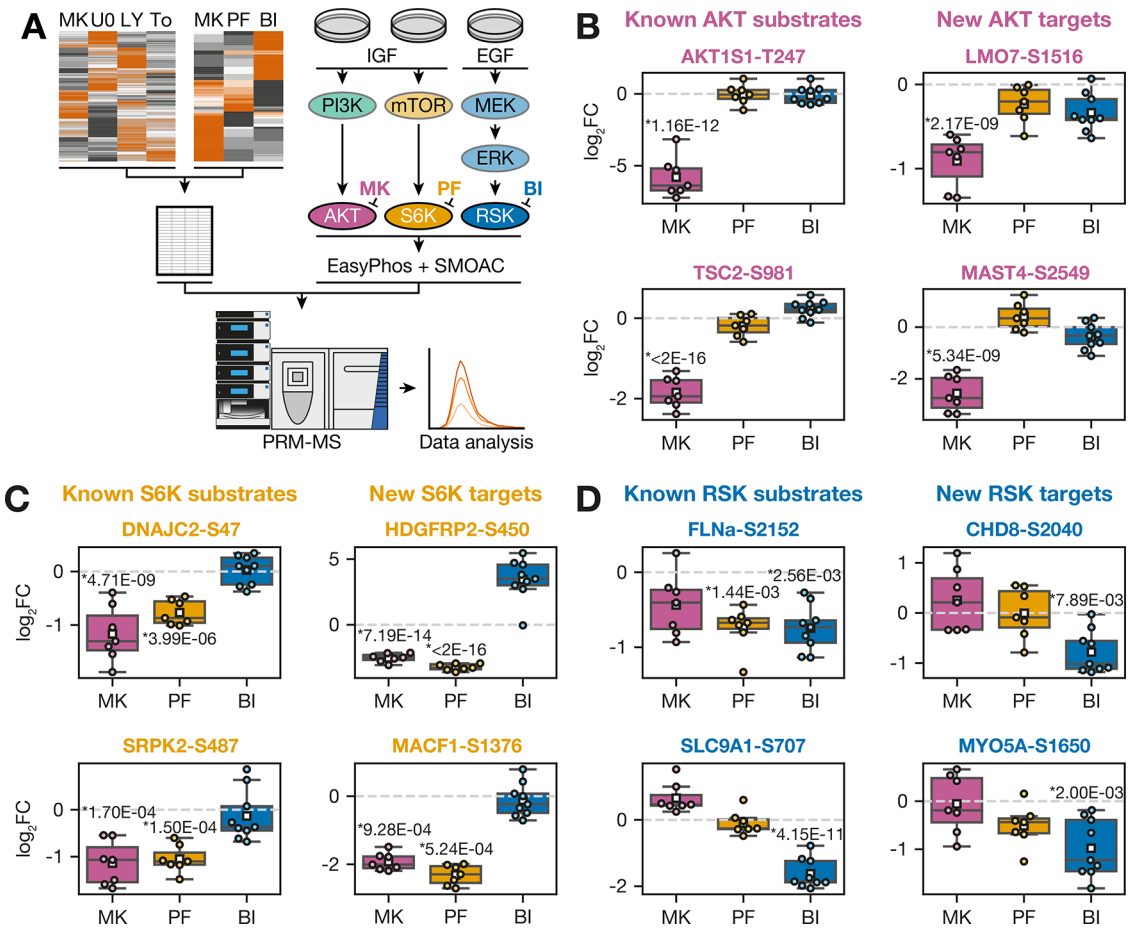

Figure 4. Study of RxRxx*p*[ST]-containing kinase targets employing PRM. (A) Contracting C2 myotubes were treated with IGF-1 or EGF for pathway stimulation and MK-2206, PF-4708671, or BI-D1870 for kinase inhibition as described for the experiment in Figure 3A. Phosphopeptide-enriched samples were analyzed using parallel reaction monitoring (PRM), with a scheduled inclusion list. PRM data were evaluated with Skyline. (B–D) MS1 peak areas of phosphopeptides were normalized to internal control phosphopeptides, and $\log_2$ fold changes (FC, fold change; inhibitor/stimulus) were calculated. Box plots show the data of selected phosphopeptides of known kinase substrates and novel targets. MK, MK-2206; PF, PF-4708671; and BI, BI-D1870.

and RAF.[41−44] In addition, KSEA showed that PF had no significant effect on AKT and RSK substrate phosphorylation, which is in line with our Western blot data (Figures 3C and S4E,F). In recent work, it has been shown that AMPKα2-S377 is a substrate of mTORC1 and involved in insulin-stimulated glucose uptake in skeletal muscle.[115] By the downregulation of AMPKα2-S377 upon MK but not PF treatment, our data confirm that AMPKα2-S377 is phosphorylated downstream of AKT but upstream of S6K (Supplemental Table 6). We found that RSK inhibition using BI led to an upregulation of ERK substrates (Figure 3C,D), which might suggest a negative feedback loop of RSK on ERK in accordance with previous studies.[116,117] KSEA further indicated that BI treatment might also affect cyclin-dependent kinase 1 (CDK1) and PKA catalytic subunit α substrate phosphorylation (Figure 3C). However, since CDK1 prefers a proline-directed recognition motif[118] and only two CDK1 substrates were affected, we concluded that this slight off-target effect of BI on CDK1 does not compromise our analysis. We further analyzed PKA substrate phosphorylation using different activators and inhibitors by immunoblotting (Figure S3D). In this analysis, we did not observe reduced phosphorylation of *bona fide* PKA substrate phosphorylation upon BI treatment, which is in line with a previous study.[116] Thus, we concluded that PKA activity is likely not affected by BI.

For further analysis, we selected each inhibitor-dependent set of significantly downregulated phosphopeptides, which exhibit the basophilic motif. Cluster analysis of these 128 significantly downregulated RxRxx*p*[ST]-containing phosphopeptides resulted in three specific kinase inhibitor-dependent regulation profiles for known and new putative AKT, RSK, and S6K substrates (Figure 3E and Supplemental Table 7). Furthermore, PCA together with annotation of known AKT, S6K, and RSK substrates revealed target candidate sets specific for each kinase (Figure 3F).

Directed MS Analysis of Putative Kinase Targets

Based on our discovery-driven phosphoproteomics data, we obtained different sets of so far unknown putative AKT-, S6K-, and RSK-dependent phosphorylation sites. To compile a joint candidate list for target-directed analysis using PRM, the RxRxx*p*[ST]-containing phosphopeptides were further filtered ($\log_2$ FC < −0.3, adjusted *p*-value <0.05 for SILAC data; $\log_2$ FC < 0, adjusted *p*-value <0.1 for label-free data) (Figure 4A, left and Supplemental Table 8). Pathway activation, kinase inhibition, and phosphopeptide enrichment were performed as for the label-free approach followed by PRM analysis (Figure 4A, right and see Figure 3A). To confirm the effectiveness and accuracy of the targeted approach, we first inspected the acquired phosphosite-resolved regulation profiles obtained for known

https://doi.org/10.1021/acs.jproteome.2c00505
J. Proteome Res. XXXX, XXX, XXX−XXX

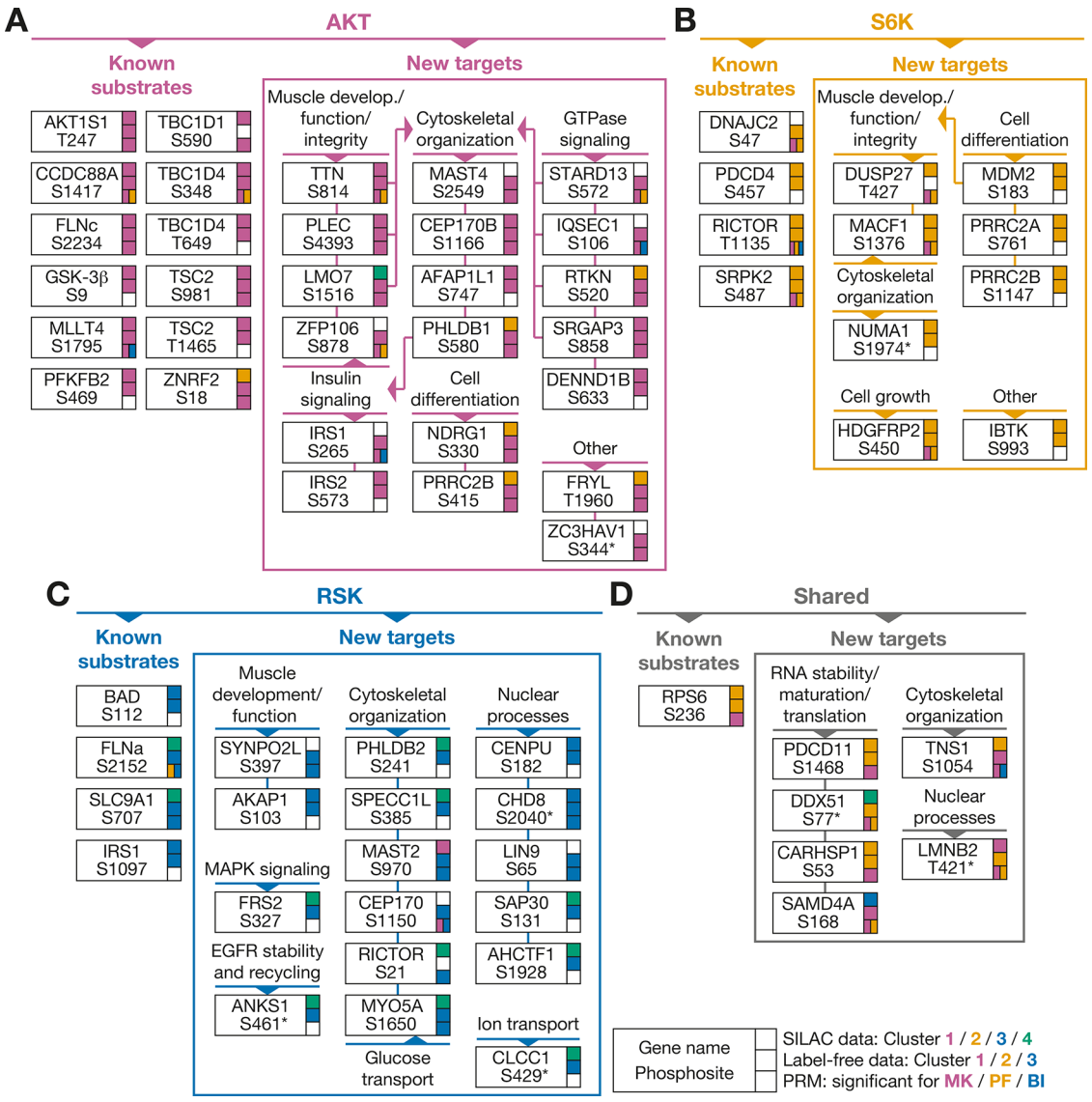

Figure 5. Compilation of AKT, S6K, and RSK phosphorylation targets confirmed in this work. Shown are known and newly identified AKT, S6K, and RSK target sites assigned to the same potential kinase group in at least two of the three phosphoproteomics experiments. If a phosphosite is part of phosphopeptides with a different multiplicity, the phosphopeptide with the lowest number of phosphosites was considered. Proteins in cluster 4 of the SILAC dataset (see Figure 2D) were deemed potential RSK targets. Phosphopeptides are color-coded with respect to their cluster membership of the two independent discovery experiments and significance in the PRM analysis. The identified target phosphosites are conserved in human, except for those sites marked (*).

kinase substrates in our list (Figure 4B–D and Supplemental Table 8). The PRM data confirmed that direct AKT substrates, such as AKT1S1-T247 and TSC2-S981, were significantly downregulated by MK only (Figure 4B). In contrast, phosphorylation levels of S6K substrates, such as DnaJ homolog subfamily C member 2 (DNAJC2)-S47 and SRSF protein kinase 2 (SRPK2)-S487, were significantly reduced by both MK and PF (Figure 4C). This finding was expected because AKT acts upstream of S6K. Filamin A (FLNa)-S2152 and sodium/hydrogen exchanger 1 (SLC9A1)-S707 are annotated as RSK and AKT substrates in the PhosphoSitePlus database.[63] Here, we show that the SLC9A1 site is specifically targeted by RSK but not AKT and S6K in skeletal myotubes (Figure 4D). Using PRM, we also validated novel targets of AKT, S6K, and RSK as exemplarily shown for LIM domain only protein 7 (LMO7)-S1516 and microtubule-associated serine/threonine-protein kinase (MAST) 4-S2549 for AKT, hepatoma-derived growth factor 2 (HDGFRP2)-S450 and microtubule-actin cross-linking factor 1 (MACF1)-S1376 for S6K, as well as chromodomain-helicase-DNA-binding protein 8 (CHD8)-S2040 and unconventional myosin-Va (MYO5A)-S1650 for RSK (Figure 4B–D and Supplemental Table 8).

We next sought to compile an overview of the reliably identified phosphorylation targets for AKT, S6K, and RSK. For this, we performed an integrative analysis of the RxRxxp[ST] phosphopeptides obtained in the (i) SILAC profiling, (ii) label-free discovery, and (iii) targeted MS study to reliably define specific kinase targets (Figure 5A–D and Supplemental Table 9). For phosphopeptides with consistent inhibitor profiles in all three datasets, kinase assignment was straightforward. For example, phosphorylation of SLIT-ROBO Rho GTPase-activating protein 3 (SRGAP3)-S858 was downregulated upon AKT inhibition in all three studies. For other kinase assignments, we applied the following criteria. First, phosphosites

https://doi.org/10.1021/acs.jproteome.2c00505
J. Proteome Res. XXXX, XXX, XXX−XXX

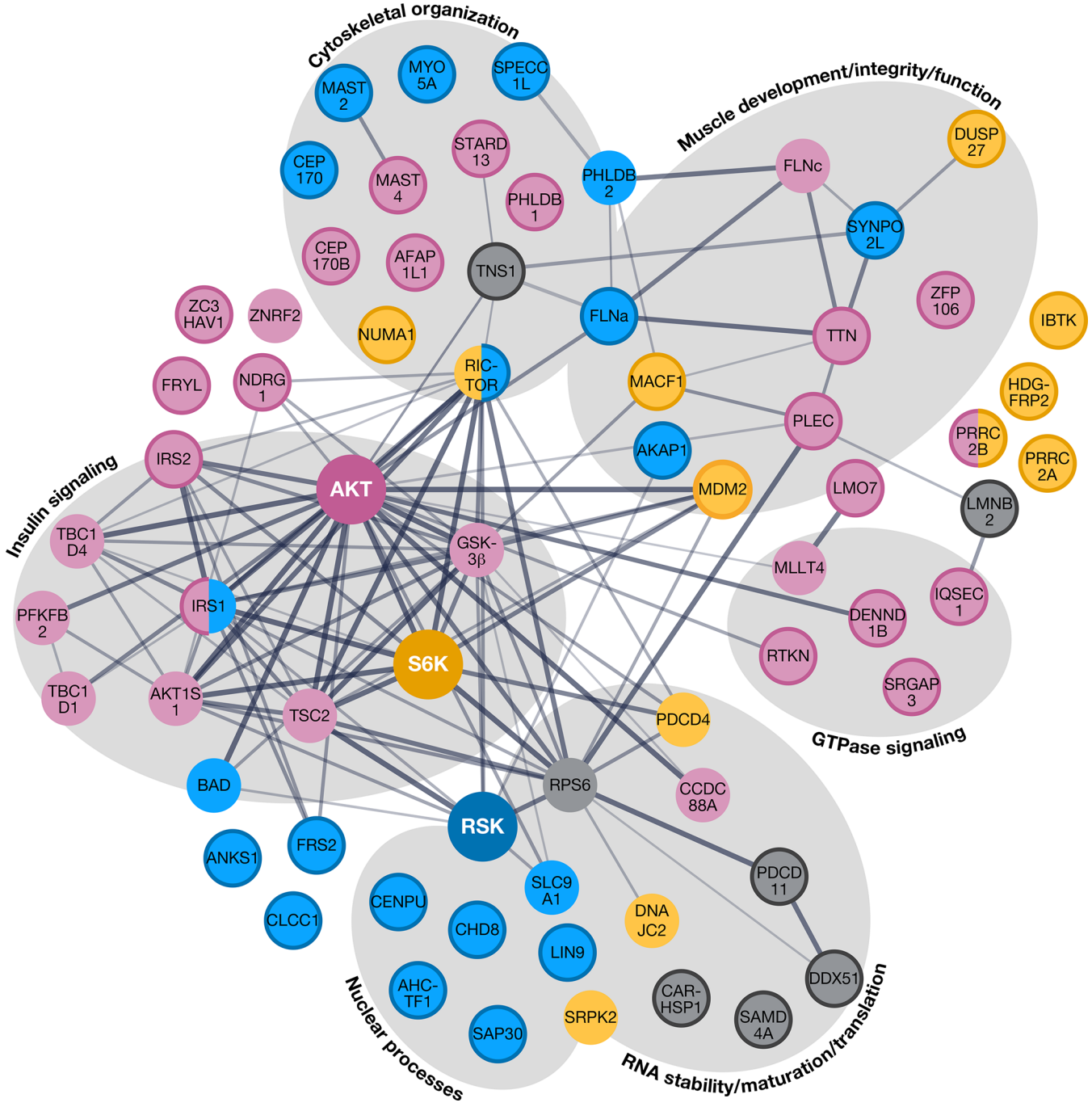

Figure 6. Functional network of validated, known, and newly identified AKT, S6K, and RSK targets. Protein network analysis was performed using the STRING database (www.string-db.org). The line width of the network represents the confidence of the reported interaction. Proteins are color-coded and grouped according to their upstream kinase and GO annotation, respectively. Red, AKT; yellow, S6K; blue, RSK; gray, shared targets; and circle with bold edging: newly identified targets.

should be mapped to the same kinase in at least two of the three phosphoproteomics experiments. Second, due to similar effects of U0 and LY on phosphopeptides present in cluster 4 of the SILAC study, these sites were considered as potential RSK targets (see Figure 2D and Supplemental Table 4). And third, phosphopeptides were deemed shared targets, if they were identified in all three studies, but the outcomes for their kinase relationships differed (Figure 5D). Our integrative analysis resulted in the assignment of 49 novel kinase targets with 19 for AKT, 8 for S6K, 16 for RSK, and 6 shared targets. Of these, more than 85% (42 out of 49) are conserved in humans (Figure 5 and Supplemental Table 9). Of the 49 novel kinase targets, 16 AKT, 3 S6K, and 7 RSK targets were corroborated *via* PRM (Figure 5A−C). In addition, our phosphoproteomics data confirm 12, 4, and 4 known AKT, S6K, and RSK substrate sites, respectively. During the course of this study, five of the novel AKT targets, namely, centrosomal protein of 170 kDa (CEP170) B-S1166, FRY-like transcription coactivator (FRYL)-T1960, plectin (PLEC)-S4393, RNA-binding protein zinc finger protein 106 (ZFP106)-S878, and IRS1-S265 (Figure 5A), have been reported as AKT substrates in breast cancer cells,[119] which underscores the validity of our data. We also provide evidence

https://doi.org/10.1021/acs.jproteome.2c00505
J. Proteome Res. XXXX, XXX, XXX−XXX

for shared kinase substrates (Figure 5D). Interestingly, proteins with confirmed or putative functions in ribosomal RNA maturation, ribosome biogenesis, mRNA stability, and mRNA translation, including programmed cell death protein 11 (PDCD11)-S1468, ATP-dependent RNA helicase DDX51-S77 calcium-regulated heat-stable protein 1 (CARHSP1)-S53, and sterile α motif domain-containing protein 4A (SAMD4A)-S168, feature shared target sites for AKT, S6K, and/or RSK, which suggests pathway-synergistic mechanisms to precisely regulate and fine-tune translation. Moreover, phosphorylation promiscuity potentially introduces a point of pathway cross talk.[120] This might well apply to the shared S6K/AKT/RSK site S1054 in tensin 1 (TNS1), which is known to link signal transduction pathways to the actin cytoskeleton.[121]

Our data reveal that all three kinases individually target numerous proteins with important roles in skeletal muscle development, functions, and/or structural integrity (Figures 5A−C and 6). Titin (TTN), which is phosphorylated by AKT at S814 (Figure 5A), links sarcomeric myosin filaments to the Z-disc[122] and functions as molecular spring to provide elasticity to muscle cells.[123] AKT also phosphorylates the cytoskeletal cross-linking protein PLEC at S4393 and the transcription factor LMO7 at S1516. PLEC is important for maintaining the desmin intermediate filament network, and loss of PLEC leads to disruption of the skeletal muscle fiber integrity and a reduced mitochondrial function.[124] LMO7 plays a role in myoblast differentiation and relocates from the nucleus to the cytoplasm during myotube formation.[125] Moreover, an upregulation of LMO7 in cells exposed to mechanical forces has been recently reported,[126] which suggests a protective role for LMO7 in withstanding mechanical forces. Thus, it will be of interest to investigate the precise function of LMO7 and whether AKT-mediated phosphorylation plays a role in the dynamic shuttling of LMO7 between the nucleus and the cytoplasm.

ZFP106 is highly abundant in skeletal muscle, and loss of ZFP106 in mice leads to muscle wasting, denervation, and premature death.[127] Here, we report ZFP106-S878 as a direct target of AKT and potentially also of S6K (Figure 5A). In addition, S6K, and likely also AKT, phosphorylate the inactive dual-specificity phosphatase 27 (DUSP27; also known as STYXL2) at T427 (Figure 5B). Loss of *dusp*27 in zebrafish results in drastic disorganization of the sarcomere, which leads to severe embryonic motility failures.[128] DUSP27 is upregulated during differentiation and most likely involved in myofiber assembly.[128] Moreover, we identified the E3 ubiquitin−protein ligase Mdm2 (MDM2)-S183 as a direct target of S6K in skeletal muscle cells, whereas human MDM2 was previously reported to be a substrate of AKT and phosphorylation was shown to initiate its translocation to the nucleus.[129−131] MDM2 plays a role in skeletal muscle regeneration and exercise-induced angiogenesis, and its deficiency elevates mitochondrial complex I activity and skeletal muscle endurance.[132−134] Furthermore, cytoplasmic MDM2 leads to oxidative stress by inhibiting localization of NADH-ubiquinone oxidoreductase 75 kDa subunit (NDUFS1) to mitochondria, thereby leading to mitochondrial respiratory defects.[135] Interestingly, our data show that RSK phosphorylates A-kinase anchor protein 1 (AKAP1)-S103 in skeletal myotubes (Figure 5C), whereas in exercising human skeletal muscle, it was identified as an AMPK target with a role in mitochondrial complex I activation by facilitating NDUFS1 mitochondrial translocation.[136,137]

Another specific RSK target is the striated muscle-specific protein synaptopodin 2-like (SYNPO2L)-S397 (Figure 5C). SYNPO2L is highly phosphorylated in contracting skeletal myotubes,[46] interacts with α-actinin at the sarcomeric Z-disc, and is crucial for striated muscle development.[138] In addition, we identified numerous cytoskeletal-associated proteins as so far unknown targets of RSK and AKT in particular (Figures 5A,C and 6). The skeletal muscle cytoskeleton is indispensable for mechanotransduction and cellular integrity upon contraction.[139,140] Abnormalities within skeletal muscle cytoskeletal organization can cause severe disorders, such as muscle dystrophies, myopathies, and atrophy.[139,141] Here, we show that the unconventional myosin MYO5A-S1650 is a phosphorylation target of RSK in skeletal myotubes (Figure 5C), whereas in adipocytes, it was identified as an AKT2 substrate, with a role in cellular GLUT4 vesicle transport.[142] In line with the central role of AKT in insulin signaling, with regulating glucose uptake[84,85] and glycogen synthesis,[25] we found that it specifically phosphorylates IRS1 at S265 and IRS2 at S573 (Figures 5A and 6). However, given that RSK specifically phosphorylates IRS1-S1097[143] and MYO5A-S1650 (Figure 5C), our data underscore an additional regulatory role of RSK in glucose metabolism in myotubes.

In skeletal muscle, microtubules are especially important for nucleus positioning, intracellular trafficking, as well as facilitating mechanical resistance and force transmission to the nucleus.[144,145] The nuclear mitotic apparatus protein 1 (NUMA1) is phosphorylated at S1974 by S6K and the CEP170 at S1150 by RSK, and both are involved in microtubule organization (Figure 5B,C).[146,147] However, their exact roles in skeletal muscle remain to be elucidated, given that the nuclear envelop rather than the centrosome functions as microtubule-organizing center in myotubes.[144] Both, MACF1 and SPECC1-like protein (SPECC1L) were shown to act on focal adhesion dynamics in keratinocytes and stabilization of microtubules in osteosarcoma cells, respectively.[148,149] We show that S6K and RSK target MACF1-S1376 and SPECC1L-S385, respectively (Figure 5B). MACF1 is especially expressed in neural, lung, and muscle cells,[150] and its loss in skeletal muscle results in impaired structures of the sarcoplasmic reticulum and mitochondria.[151] AKT and RSK phosphorylate MAST4-S2549 and MAST2-S970, respectively (Figure 5A,C). Whereas MAST4 is poorly characterized, MAST2 links the dystrophin complex with the microtubule network.[152] Furthermore, AKT and RSK phosphorylate pleckstrin homology-like domain family B member (PHLDB) 1 at S580 and PHLDB2 at S241, respectively. PHLDB1 and PHLDB2 play a role in the localization of laminin receptor integrins at the basal cortex of epithelial cells[153] and integrin internalization,[154] whereas PHLDB1 is important for AKT-mediated GLUT4 translocation upon insulin stimulation in adipocytes[155] and PHLDB2 is involved in stabilization of microtubules.[156] Furthermore, AKT mediates the phosphorylation of the actin filament-associated protein 1-like 1 (AFAP1L1)-S747, which is associated with accelerated tumor growth and enhanced cell invasion.[157,158]

In line with the known property of RSK to translocate to the nucleus,[159] we identified different nuclear targets, *e.g.*, with functions in chromatin segregation and/or transcription, specifically for RSK (Figures 5C and 6). Distinct from RSK and also S6K, we found that AKT specifically targets several proteins involved in GTPase signaling, *i.e.*, START domain-containing protein 13 (STARD13)-S572, SRGAP3-S858, DENN domain-containing protein 1B (DENND1B)-S633 and IQ motif and SEC7 domain-containing protein 1 (IQSEC1)-S106 (Figures 5A and 6). STARD13 and SRGAP3 are GTPase-

https://doi.org/10.1021/acs.jproteome.2c00505
J. Proteome Res. XXXX, XXX, XXX−XXX

activating proteins for the small GTPases ras homolog family member A (RhoA) and cell division cycle 42 (Cdc42)[160] and for Rac1,[161] respectively. Whereas STARD13 was suggested to block proliferation *via* inhibition of RhoA[162] and was shown to regulate insulin secretion by cytoskeletal remodeling,[163] SRGAP3 inhibits Rac1 for actin cytoskeleton reorganization.[161] In neurons, SRGAP3 was shown to be activated by PKA-mediated phosphorylation at S858.[164] DENND1B and IQSEC1 are guanine nucleotide exchange factors for the small GTPases Rab35[165] and ADP ribosylation factor 5/6 (ARF5/6),[166] respectively, with functions in cytoskeletal organization and vesicular trafficking.[167−169] Furthermore, *via* ARF5/6 activation, IQSEC1 promotes AKT signaling in tumor growth and invasion.[166]

CONCLUSIONS

This study provides a facet of the intertwined PI3K-AKT-mTOR-S6K and RAF-MEK-ERK-RSK signaling networks in contracting skeletal muscle cells. Our phosphoproteomics data provide a valuable resource for functional studies on AKT, S6K, and RSK targets at a phosphosite-specific level. Quantitative phosphoproteomics profiling in combination with computational data evaluation proved to be a dependable approach for establishing kinase inhibitor-dependent regulation profiles to delineate a AKT, S6K, and RSK target landscape, even though they share the same basophilic recognition motif. Furthermore, we advocate the integration of phosphoproteomics data from kinase inhibition at different levels of the pathway to identify high-confidence kinase targets and to reveal cross talk and feedback loops between signaling pathways. To facilitate this multifaceted kinase inhibition approach, we employed a cell culture-based C2 myotube model system. Thus, some of the findings reported here might not translate into native skeletal muscle or other cell types that differ in their expression and/or localization profiles of AKT, S6K, and RSK isoforms and target proteins. In addition, potential off-target effects of kinase inhibitors need to be taken into consideration. Thus, kinase−substrate relationships should be independently validated, for example, using RNAi-mediated knockdown, gene editing or chemical genetic approaches for targeting protein kinases, *in vitro* kinase assays, and/or *in vivo* models. Finally, the reported phosphosite localizations and quantifications in this study are computationally assessed, and their accuracy depend on the abundance, ionization efficiency, and fragmentation behavior of the respective phosphopeptides. However, with regard to the reported kinase targets, we mitigated this issue by assessing phosphosite data from three different phosphoproteomics experiments in combination with different phosphopeptide enrichment methods, global and targeted MS technology, and applying the basophilic kinase recognition motif for down-regulated phosphopeptides as an additional filter. In sum, the 49 so far unknown phosphorylation targets reported in this work provide a valuable resource for expanding the current knowledge about how AKT, S6K, and RSK control the fate and functions of skeletal muscle cells.

ASSOCIATED CONTENT

Supporting Information

The Supporting Information is available free of charge at https://pubs.acs.org/doi/10.1021/acs.jproteome.2c00505.

Supplemental experimental section; antibodies used in this study (Supplemental Experimental Table S1); uncropped Western blot images of Figure 1 (Experimental Figure 1a−e); uncropped Western blot and Coomassie images of Figure S4 (Supplemental Experimental Figure 2a−d); mapping of PI3K-AKT-mTOR-S6K and RAF-MEK-ERK-RSK pathways (Figure S1); evaluation of the global quantitative phosphoproteome after pathway inhibition using MK-2206, LY294002, U0126, and Torin1 (Figure S2); enriched motifs within downregulated phosphopeptides upon PI3K-AKT-mTOR-S6K and RAF-MEK-ERK-RSK pathway inhibition (Figure S3); activation and inhibition time course for AKT, S6K, and RSK signaling by pharmacological intervention (Figure S4); evaluation of the global label-free phosphoproteome after combined pathway activation and inhibition (Figure S5) (PDF)

Proof of concept based on known kinase−substrate relationships (Supplemental Table 1); data of the global MK/U0/LY/To SILAC phosphoproteomics experiment (Supplemental Table 2); evaluation of regulated motifs and kinases in the global MK/U0/LY/To SILAC phosphoproteomics experiment (Supplemental Table 3); motif clusterings of the global MK/U0/LY/To SILAC phosphoproteomics experiment (Supplemental Table 4); text mining results for the RxRxxp[ST] clustering of the global MK/U0/LY/To SILAC phosphoproteomics experiment (Supplemental Table 5); data of the global label-free MK/BI/PF phosphoproteomics experiment (Supplemental Table 6); KSEA and motif clustering of the label-free MK/PF/BI phosphoproteomics experiment (Supplemental Table 7); quantitative MS data of the kinase target validation assay using targeted MS (Supplemental Table 8); summary of the RxRxxp[ST]-containing phosphopeptides (Supplemental Table 9) (ZIP)

AUTHOR INFORMATION

Corresponding Author

Bettina Warscheid − *Biochemistry and Functional Proteomics, Institute of Biology II, Faculty of Biology, University of Freiburg, 79104 Freiburg, Germany; Biochemistry II, Theodor Boveri-Institute, Biocenter, University of Würzburg, 97074 Würzburg, Germany; Signalling Research Centres BIOSS and CIBSS, University of Freiburg, 79104 Freiburg, Germany;* orcid.org/0000-0001-5096-1975; Email: bettina.warscheid@uni-wuerzburg.de

Authors

Anna L. Fricke − *Biochemistry and Functional Proteomics, Institute of Biology II, Faculty of Biology, University of Freiburg, 79104 Freiburg, Germany; Biochemistry II, Theodor Boveri-Institute, Biocenter, University of Würzburg, 97074 Würzburg, Germany*

◆**Wignand W. D. Mühlhäuser** − *Biochemistry and Functional Proteomics, Institute of Biology II, Faculty of Biology, University of Freiburg, 79104 Freiburg, Germany*

◆**Lena Reimann** − *Biochemistry and Functional Proteomics, Institute of Biology II, Faculty of Biology, University of Freiburg, 79104 Freiburg, Germany*

Johannes P. Zimmermann − *Biochemistry II, Theodor Boveri-Institute, Biocenter, University of Würzburg, 97074 Würzburg, Germany;* orcid.org/0000-0001-5692-2096

https://doi.org/10.1021/acs.jproteome.2c00505
J. Proteome Res. XXXX, XXX, XXX−XXX

Christa Reichenbach − *Biochemistry and Functional Proteomics, Institute of Biology II, Faculty of Biology, University of Freiburg, 79104 Freiburg, Germany*
Bettina Knapp − *Biochemistry and Functional Proteomics, Institute of Biology II, Faculty of Biology, University of Freiburg, 79104 Freiburg, Germany*
◆**Christian D. Peikert** − *Biochemistry and Functional Proteomics, Institute of Biology II, Faculty of Biology, University of Freiburg, 79104 Freiburg, Germany*
Alexander M. Heberle − *Institute of Biochemistry and Center for Molecular Biosciences Innsbruck, University of Innsbruck, 6020 Innsbruck, Austria;* orcid.org/0000-0001-6414-8707
Erik Faessler − *Jena University Language & Information Engineering (JULIE) Lab, Friedrich Schiller University Jena, 07743 Jena, Germany;* orcid.org/0000-0003-1193-5103
Sascha Schäuble − *Jena University Language & Information Engineering (JULIE) Lab, Friedrich Schiller University Jena, 07743 Jena, Germany; Systems Biology and Bioinformatics Unit, Leibniz Institute for Natural Product Research and Infection Biology—Leibniz-HKI, 07745 Jena, Germany;* orcid.org/0000-0003-3862-6546
Udo Hahn − *Jena University Language & Information Engineering (JULIE) Lab, Friedrich Schiller University Jena, 07743 Jena, Germany*
Kathrin Thedieck − *Institute of Biochemistry and Center for Molecular Biosciences Innsbruck, University of Innsbruck, 6020 Innsbruck, Austria; Department of Pediatrics, Section Systems Medicine of Metabolism and Signaling, University of Groningen, University Medical Center Groningen, Groningen 9700 RB, The Netherlands; Department for Neuroscience, School of Medicine and Health Sciences, Carl von Ossietzky University Oldenburg, Oldenburg 26129, Germany;* orcid.org/0000-0002-9069-2930
Gerald Radziwill − *Biochemistry and Functional Proteomics, Institute of Biology II, Faculty of Biology, University of Freiburg, 79104 Freiburg, Germany; Signalling Research Centres BIOSS and CIBSS, University of Freiburg, 79104 Freiburg, Germany*

Complete contact information is available at: https://pubs.acs.org/10.1021/acs.jproteome.2c00505

Author Contributions

A.L.F. performed all phosphoproteomics experiments with the help of L.R. and support of C.R., B.K., and A.M.H. Bioinformatics analyses were performed by W.W.D.M., J.P.Z., C.D.P, and A.L.F. and text mining by E.F., S.S., and U.H. All authors analyzed data, designed, and interpreted experiments. B.W. supervised the study and conceived the project. B.W. and A.L.F wrote the manuscript with the input of all other authors. All authors have given approval to the final version of the manuscript.

Funding

This work was supported by the Deutsche Forschungsgemeinschaft (DFG, German Research Foundation) FOR 2743 (WA1598/6), TRR 130, and Germany's Excellence Strategy (CIBSS—EXC-2189—project ID 390939984). E.F. and U.H. are supported by BMBF within the SMITH project under grant 01ZZ1803G.

Notes

The authors declare no competing financial interest.

◆W.W.D.M., L.R., and C.D.P. no longer work in academia.

■ ACKNOWLEDGMENTS

The authors thank the PRIDE team for ProteomeXchange Consortium data deposition, Vagisha Sharma, and the PanoramaWeb team for their support with data deposition to Panorama Public and Dieter Fürst (University of Bonn) for scientific support and discussions. Work included in this study has been performed in partial fulfillment of the doctoral thesis of A.L.F. at the University of Freiburg and J.P.Z. at the University of Würzburg.

■ ABBREVIATIONS

ACN, acetonitrile; AKT1S1, AKT1 substrate 1; AMPK, AMP-activated kinase; ARF5/6, ADP ribosylation factor 5/6; BAD, Bcl2-associated agonist of cell death; BI, BI-D1870; CDK1, cyclin-dependent kinase 1; CEP170(B), centrosomal protein of 170 kDa (B); CHD8, chromodomain-helicase-DNA-binding protein 8; DENND1B, DENN domain-containing protein 1B; DMSO, dimethyl sulfoxide; DNAJC2, DnaJ homolog subfamily C member 2; DUSP27, inactive dual-specificity phosphatase 27 (=STYXL2); eEF2(K), eukaryotic elongation factor 2 (kinase); EGF, epidermal growth factor; eIF-4B, eukaryotic initiation factor 4B; EPS, electrical pulse stimulation; ERK1/2, extracellular signal-regulated kinase 1/2; FA, formic acid; FC, fold change; FCS, fetal calf serum; FDR, false discovery rate; FI, Forskolin and IBMX; FLNa/c, filamin A/C; GO, gene ontology; GSK-3, glycogen synthase kinase-3; HDGFRP2, hepatoma-derived growth factor 2; hpH RP, high pH reversed-phase; iBAQ, intensity-based absolute quantification; IGF-1, insulin-like growth factor 1; IMAC, immobilized metal affinity chromatography; IRS1/2, insulin receptor substrate 1/2; IT, ion time; KSEA, kinase−substrate enrichment analysis; LC, liquid chromatography; LMO7, LIM domain only protein 7; LY, LY294002; IQSEC1, IQ motif and SEC7 domain-containing protein 1; MACF1, microtubule-actin cross-linking factor 1; MAPK, mitogen-activated protein kinase; MAST2/4, microtubule-associated Ser/Thr-protein kinase 2/4; MEK1/2, mitogen-activated protein kinase kinase 1/2; MDM2, E3 ubiquitin−protein ligase Mdm2; MK, MK-2206; MS, mass spectrometry; MYO5A, unconventional myosin-Va; mTOR-(C1/2), mechanistic target of rapamycin (complex 1/2); NDUFS1, NADH−ubiquinone oxidoreductase 75 kDa subunit; NEAA, non-essential amino acids; PCA, principal component analysis; PC1/2, principal component 1/2; PDK1/2, 3-phosphoinositide-dependent protein kinase 1/2; PF, PF-4708671; PHLDB1/2, pleckstrin homology-like domain family B member 1/2; PI3K, phosphoinositide 3-kinase; PKA, protein kinase A; PLEC, plectin; PRM, parallel reaction monitoring; Rac1, Rac family small GTPase 1; RhoA, ras homolog family member A; RICTOR, RPTOR independent companion of MTOR complex 2; RPS6, 40S ribosomal protein S6; RSK, 90 kDa ribosomal protein S6 kinase; RT, room temperature; SDS, sodium dodecyl sulfate; SILAC, stable isotope labeling by amino acids in cell culture; SMOAC, sequential metal oxide affinity chromatography; SLC9A1, sodium/hydrogen exchanger 1; SPECC1L, SPECC1-like protein; SRGAP3, SLIT-ROBO Rho GTPase-activating protein 3; SRPK2, SRSF protein kinase 2; STARD13, START domain-containing protein 13; SYNPO2L, synaptopodin 2-like; S6K, 70 kDa ribosomal protein S6 kinase; TFA, trifluoroacetic acid; TiO_2, titanium dioxide; To, Torin1;

https://doi.org/10.1021/acs.jproteome.2c00505
J. Proteome Res. XXXX, XXX, XXX−XXX

TSC2, TSC complex subunit 2; U0, U0126; ZFP106, RNA-binding protein zinc finger protein 106

REFERENCES

(1) Jiang, B.-H.; Aoki, M.; Zheng, J. Z.; Li, J.; Vogt, P. K. Myogenic Signaling of Phosphatidylinositol 3-Kinase Requires the Serine-Threonine Kinase Akt/Protein Kinase B. *Proc. Natl. Acad. Sci. U.S.A.* **1999**, *96*, 2077−2081.

(2) Gardner, S.; Anguiano, M.; Rotwein, P. Defining Akt Actions in Muscle Differentiation. *Am. J. Physiol.: Cell Physiol.* **2012**, *303*, C1292−C1300.

(3) Coolican, S. A.; Samuel, D. S.; Ewton, D. Z.; McWade, F. J.; Florini, J. R. The Mitogenic and Myogenic Actions of Insulin-like Growth Factors Utilize Distinct Signaling Pathways. *J. Biol. Chem.* **1997**, *272*, 6653−6662.

(4) Bennett, A. M.; Tonks, N. K. Regulation of Distinct Stages of Skeletal Muscle Differentiation by Mitogen-Activated Protein Kinases. *Science* **1997**, *278*, 1288−1291.

(5) Gredinger, E.; Gerber, A. N.; Tamir, Y.; Tapscott, S. J.; Bengal, E. Mitogen-Activated Protein Kinase Pathway Is Involved in the Differentiation of Muscle Cells. *J. Biol. Chem.* **1998**, *273*, 10436−10444.

(6) Jaiswal, N.; Gavin, M. G.; Quinn, W. J.; Luongo, T. S.; Gelfer, R. G.; Baur, J. A.; Titchenell, P. M. The Role of Skeletal Muscle Akt in the Regulation of Muscle Mass and Glucose Homeostasis. *Mol. Metab.* **2019**, *28*, 1−13.

(7) Rommel, C.; Bodine, S. C.; Clarke, B. A.; Rossman, R.; Nunez, L.; Stitt, T. N.; Yancopoulos, G. D.; Glass, D. J. Mediation of IGF-1-Induced Skeletal Myotube Hypertrophy by PI(3)K/Akt/MTOR and PI(3)K/Akt/GSK3 Pathways. *Nat. Cell Biol.* **2001**, *3*, 1009−1013.

(8) Bodine, S. C.; Stitt, T. N.; Gonzalez, M.; Kline, W. O.; Stover, G. L.; Bauerlein, R.; Zlotchenko, E.; Scrimgeour, A.; Lawrence, J. C.; Glass, D. J.; Yancopoulos, G. D. Akt/MTOR Pathway Is a Crucial Regulator of Skeletal Muscle Hypertrophy and Can Prevent Muscle Atrophy in Vivo. *Nat. Cell Biol.* **2001**, *3*, 1014−1019.

(9) Lai, K.-M. V.; Gonzalez, M.; Poueymirou, W. T.; Kline, W. O.; Na, E.; Zlotchenko, E.; Stitt, T. N.; Economides, A. N.; Yancopoulos, G. D.; Glass, D. J. Conditional Activation of Akt in Adult Skeletal Muscle Induces Rapid Hypertrophy. *Mol. Cell. Biol.* **2004**, *24*, 9295−9304.

(10) Schiaffino, S.; Mammucari, C. Regulation of Skeletal Muscle Growth by the IGF1-Akt/PKB Pathway: Insights from Genetic Models. *Skeletal Muscle* **2011**, *1*, No. 4.

(11) Shi, H.; Scheffler, J. M.; Pleitner, J. M.; Zeng, C.; Park, S.; Hannon, K. M.; Grant, A. L.; Gerrard, D. E. Modulation of Skeletal Muscle Fiber Type by Mitogen-activated Protein Kinase Signaling. *FASEB J.* **2008**, *22*, 2990−3000.

(12) Hamdi, M. M.; Mutungi, G. Dihydrotestosterone Activates the MAPK Pathway and Modulates Maximum Isometric Force through the EGF Receptor in Isolated Intact Mouse Skeletal Muscle Fibres. *J. Physiol.* **2010**, *588*, 511−525.

(13) Ciano, M.; Mantellato, G.; Connolly, M.; Paul-Clark, M.; Willis-Owen, S.; Moffatt, M. F.; Cookson, W. O. C. M.; Mitchell, J. A.; Polkey, M. I.; Hughes, S. M.; Kemp, P. R.; Natanek, S. A. EGF Receptor (EGFR) Inhibition Promotes a Slow-Twitch Oxidative, over a Fast-Twitch, Muscle Phenotype. *Sci. Rep.* **2019**, *9*, No. 9218.

(14) Baffi, T. R.; Newton, A. C. MTOR Regulation of AGC Kinases: New Twist to an Old Tail. *Mol. Pharmacol.* **2022**, *101*, 213−218.

(15) Mora, A.; Komander, D.; van Aalten, D. M. F.; Alessi, D. R. PDK1, the Master Regulator of AGC Kinase Signal Transduction. *Semin. Cell Dev. Biol.* **2004**, *15*, 161−170.

(16) Peterson, R. T.; Schreiber, S. L. Kinase Phosphorylation: Keeping It All in the Family. *Curr. Biol.* **1999**, *9*, R521−R524.

(17) Pearce, L. R.; Komander, D.; Alessi, D. R. The Nuts and Bolts of AGC Protein Kinases. *Nat. Rev. Mol. Cell Biol.* **2010**, *11*, 9−22.

(18) Moritz, A.; Li, Y.; Guo, A.; Villén, J.; Wang, Y.; MacNeill, J.; Kornhauser, J.; Sprott, K.; Zhou, J.; Possemato, A.; Ren, J. M.; Hornbeck, P.; Cantley, L. C.; Gygi, S. P.; Rush, J.; Comb, M. J. Akt-RSK-S6 Kinase Signaling Networks Activated by Oncogenic Receptor Tyrosine Kinases. *Sci. Signaling* **2010**, *3*, No. ra64.

(19) Manning, B. D.; Cantley, L. C. AKT/PKB Signaling: Navigating Downstream. *Cell* **2007**, *129*, 1261−1274.

(20) Alessi, D. R.; Andjelkovic, M.; Caudwell, B.; Cron, P.; Morrice, N.; Cohen, P.; Hemmings, B. A. Mechanism of Activation of Protein Kinase B by Insulin and IGF-1. *EMBO J.* **1996**, *15*, 6541−6551.

(21) Sarbassov, D. D.; Guertin, D. A.; Ali, S. M.; Sabatini, D. M. Phosphorylation and Regulation of Akt/PKB by the Rictor-MTOR Complex. *Science* **2005**, *307*, 1098−1101.

(22) Cameron, A. J. M.; Linch, M. D.; Saurin, A. T.; Escribano, C.; Parker, P. J. MTORC2 Targets AGC Kinases through Sin1-Dependent Recruitment. *Biochem. J.* **2011**, *439*, 287−297.

(23) Datta, S. R.; Dudek, H.; Tao, X.; Masters, S.; Fu, H.; Gotoh, Y.; Greenberg, M. E. Akt Phosphorylation of BAD Couples Survival Signals to the Cell-Intrinsic Death Machinery. *Cell* **1997**, *91*, 231−241.

(24) Rylatt, D. B.; Aitken, A.; Bilham, T.; Condon, G. D.; Embi, N.; Cohen, P. Glycogen Synthase from Rabbit Skeletal Muscle. Amino Acid Sequence at the Sites Phosphorylated by Glycogen Synthase Kinase-3, and Extension of the N-Terminal Sequence Containing the Site Phosphorylated by Phosphorylase Kinase. *Eur. J. Biochem.* **1980**, *107*, 529−537.

(25) Cross, D. A. E.; Alessi, D. R.; Cohen, P.; Andjelkovich, M.; Hemmings, B. A. Inhibition of Glycogen Synthase Kinase-3 by Insulin Mediated by Protein Kinase B. *Nature* **1995**, *378*, 785−789.

(26) Roux, P. P.; Ballif, B. A.; Anjum, R.; Gygi, S. P.; Blenis, J. Tumor-Promoting Phorbol Esters and Activated Ras Inactivate the Tuberous Sclerosis Tumor Suppressor Complex via P90 Ribosomal S6 Kinase. *Proc. Natl. Acad. Sci. U.S.A.* **2004**, *101*, 13489−13494.

(27) Kovacina, K. S.; Park, G. Y.; Bae, S. S.; Guzzetta, A. W.; Schaefer, E.; Birnbaum, M. J.; Roth, R. A. Identification of a Proline-Rich Akt Substrate as a 14-3-3 Binding Partner. *J. Biol. Chem.* **2003**, *278*, 10189−10194.

(28) Burnett, P. E.; Barrow, R. K.; Cohen, N. A.; Snyder, S. H.; Sabatini, D. M. RAFT1 Phosphorylation of the Translational Regulators P70 S6 Kinase and 4E-BP1. *Proc. Natl. Acad. Sci. U.S.A.* **1998**, *95*, 1432−1437.

(29) Pullen, N.; Dennis, P. B.; Andjelkovic, M.; Dufner, A.; Kozma, S. C.; Hemmings, B. A.; Thomas, G. Phosphorylation and Activation of P70 S6k by PDK1. *Science* **1998**, *279*, 707−710.

(30) Chauvin, C.; Koka, V.; Nouschi, A.; Mieulet, V.; Hoareau-Aveilla, C.; Dreazen, A.; Cagnard, N.; Carpentier, W.; Kiss, T.; Meyuhas, O.; Pende, M. Ribosomal Protein S6 Kinase Activity Controls the Ribosome Biogenesis Transcriptional Program. *Oncogene* **2014**, *33*, 474−483.

(31) Holz, M. K.; Ballif, B. A.; Gygi, S. P.; Blenis, J. MTOR and S6K1 Mediate Assembly of the Translation Preinitiation Complex through Dynamic Protein Interchange and Ordered Phosphorylation Events. *Cell* **2005**, *123*, 569−580.

(32) Raught, B.; Peiretti, F.; Gingras, A.-C.; Livingstone, M.; Shahbazian, D.; Mayeur, G. L.; Polakiewicz, R. D.; Sonenberg, N.; Hershey, J. W. B. Phosphorylation of Eucaryotic Translation Initiation Factor 4B Ser422 Is Modulated by S6 Kinases. *EMBO J.* **2004**, *23*, 1761−1769.

(33) Wang, X.; Li, W.; Williams, M.; Terada, N.; Alessi, D. R.; Proud, C. G. Regulation of Elongation Factor 2 Kinase by P90RSK1 and P70 S6 Kinase. *EMBO J.* **2001**, *20*, 4370−4379.

(34) Raman, M.; Chen, W.; Cobb, M. H. Differential Regulation and Properties of MAPKs. *Oncogene* **2007**, *26*, 3100−3112.

(35) Anjum, R.; Blenis, J. The RSK Family of Kinases: Emerging Roles in Cellular Signalling. *Nat. Rev. Mol. Cell Biol.* **2008**, *9*, 747−758.

(36) Shimamura, A.; Ballif, B. A.; Richards, S. A.; Blenis, J. Rsk1 Mediates a MEK−MAP Kinase Cell Survival Signal. *Curr. Biol.* **2000**, *10*, 127−135.

(37) Roux, P. P.; Shahbazian, D.; Vu, H.; Holz, M. K.; Cohen, M. S.; Taunton, J.; Sonenberg, N.; Blenis, J. RAS/ERK Signaling Promotes Site-Specific Ribosomal Protein S6 Phosphorylation via RSK and Stimulates Cap-Dependent Translation. *J. Biol. Chem.* **2007**, *282*, 14056−14064.

(38) Zhang, J.; Gao, Z.; Yin, J.; Quon, M. J.; Ye, J. S6K Directly Phosphorylates IRS-1 on Ser-270 to Promote Insulin Resistance in

https://doi.org/10.1021/acs.jproteome.2c00505
J. Proteome Res. XXXX, XXX, XXX−XXX

Response to TNF-α Signaling through IKK2. *J. Biol. Chem.* **2008**, *283*, 35375−35382.
(39) Treins, C.; Warne, P. H.; Magnuson, M. A.; Pende, M.; Downward, J. Rictor Is a Novel Target of P70 S6 Kinase-1. *Oncogene* **2010**, *29*, 1003−1016.
(40) Dibble, C. C.; Asara, J. M.; Manning, B. D. Characterization of Rictor Phosphorylation Sites Reveals Direct Regulation of MTOR Complex 2 by S6K1. *Mol. Cell. Biol.* **2009**, *29*, 5657−5670.
(41) Rommel, C.; Clarke, B. A.; Zimmermann, S.; Nuñez, L.; Rossman, R.; Reid, K.; Moelling, K.; Yancopoulos, G. D.; Glass, D. J. Differentiation Stage-Specific Inhibition of the Raf-MEK-ERK Pathway by Akt. *Science* **1999**, *286*, 1738−1741.
(42) Zimmermann, S.; Moelling, K. Phosphorylation and Regulation of Raf by Akt (Protein Kinase B). *Science* **1999**, *286*, 1741−1744.
(43) Moelling, K.; Schad, K.; Bosse, M.; Zimmermann, S.; Schweneker, M. Regulation of Raf-Akt Crosstalk. *J. Biol. Chem.* **2002**, *277*, 31099−31106.
(44) Reusch, H. P.; Zimmermann, S.; Schaefer, M.; Paul, M.; Moelling, K. Regulation of Raf by Akt Controls Growth and Differentiation in Vascular Smooth Muscle Cells. *J. Biol. Chem.* **2001**, *276*, 33630−33637.
(45) Ong, S.-E.; Blagoev, B.; Kratchmarova, I.; Kristensen, D. B.; Steen, H.; Pandey, A.; Mann, M. Stable Isotope Labeling by Amino Acids in Cell Culture, SILAC, as a Simple and Accurate Approach to Expression Proteomics. *Mol. Cell. Proteomics* **2002**, *1*, 376−386.
(46) Reimann, L.; Wiese, H.; Leber, Y.; Schwäble, A. N.; Fricke, A. L.; Rohland, A.; Knapp, B.; Peikert, C. D.; Drepper, F.; van der Ven, P. F. M.; Radziwill, G.; Fürst, D. O.; Warscheid, B. Myofibrillar Z-Discs Are a Protein Phosphorylation Hot Spot with Protein Kinase C (PKCα) Modulating Protein Dynamics. *Mol. Cell. Proteomics* **2017**, *16*, 346−367.
(47) Reimann, L.; Schwäble, A. N.; Fricke, A. L.; Mühlhäuser, W. W. D.; Leber, Y.; Lohanadan, K.; Puchinger, M. G.; Schäuble, S.; Faessler, E.; Wiese, H.; Reichenbach, C.; Knapp, B.; Peikert, C. D.; Drepper, F.; Hahn, U.; Kreutz, C.; van der Ven, P. F. M.; Radziwill, G.; Djinović-Carugo, K.; Fürst, D. O.; Warscheid, B. Phosphoproteomics Identifies Dual-Site Phosphorylation in an Extended Basophilic Motif Regulating FILIP1-Mediated Degradation of Filamin-C. *Commun. Biol.* **2020**, *3*, No. 253.
(48) Humphrey, S. J.; Karayel, O.; James, D. E.; Mann, M. High-Throughput and High-Sensitivity Phosphoproteomics with the EasyPhos Platform. *Nat. Protoc.* **2018**, *13*, 1897−1916.
(49) Choi, J.; Snovida, S. I.; Bomgarden, R.; Rogers, J. C. In *Sequential Enrichment from Metal Oxide Affinity Chromatography (SMOAC), A Phosphoproteomics Strategy for the Separation of Multiply Phosphorylated from Monophosphorylated Peptides*, 65th ASMS Conference on Mass Spectrometry and Allied Topics, 2017.
(50) MacLean, B.; Tomazela, D. M.; Shulman, N.; Chambers, M.; Finney, G. L.; Frewen, B.; Kern, R.; Tabb, D. L.; Liebler, D. C.; MacCoss, M. J. Skyline: An Open Source Document Editor for Creating and Analyzing Targeted Proteomics Experiments. *Bioinformatics* **2010**, *26*, 966−968.
(51) Cox, J.; Mann, M. MaxQuant Enables High Peptide Identification Rates, Individualized p.p.b.-Range Mass Accuracies and Proteome-Wide Protein Quantification. *Nat. Biotechnol.* **2008**, *26*, 1367−1372.
(52) Cox, J.; Neuhauser, N.; Michalski, A.; Scheltema, R. A.; Olsen, J. V.; Mann, M. Andromeda: A Peptide Search Engine Integrated into the MaxQuant Environment. *J. Proteome Res.* **2011**, *10*, 1794−1805.
(53) Schwanhäusser, B.; Busse, D.; Li, N.; Dittmar, G.; Schuchhardt, J.; Wolf, J.; Chen, W.; Selbach, M. Global Quantification of Mammalian Gene Expression Control. *Nature* **2011**, *473*, 337−342.
(54) Schilling, B.; Rardin, M. J.; MacLean, B. X.; Zawadzka, A. M.; Frewen, B. E.; Cusack, M. P.; Sorensen, D. J.; Bereman, M. S.; Jing, E.; Wu, C. C.; Verdin, E.; Kahn, C. R.; MacCoss, M. J.; Gibson, B. W. Platform-Independent and Label-Free Quantitation of Proteomic Data Using MS1 Extracted Ion Chromatograms in Skyline: Application to Protein Acetylation and Phosphorylation. *Mol. Cell. Proteomics* **2012**, *11*, 202−214.
(55) Perez-Riverol, Y.; Csordas, A.; Bai, J.; Bernal-Llinares, M.; Hewapathirana, S.; Kundu, D. J.; Inuganti, A.; Griss, J.; Mayer, G.; Eisenacher, M.; Pérez, E.; Uszkoreit, J.; Pfeuffer, J.; Sachsenberg, T.; Yilmaz, S.; Tiwary, S.; Cox, J.; Audain, E.; Walzer, M.; Jarnuczak, A. F.; Ternent, T.; Brazma, A.; Vizcaíno, J. A. The PRIDE Database and Related Tools and Resources in 2019: Improving Support for Quantification Data. *Nucleic Acids Res.* **2019**, *47*, D442−D450.
(56) Sharma, V.; Eckels, J.; Taylor, G. K.; Shulman, N. J.; Stergachis, A. B.; Joyner, S. A.; Yan, P.; Whiteaker, J. R.; Halusa, G. N.; Schilling, B.; Gibson, B. W.; Colangelo, C. M.; Paulovich, A. G.; Carr, S. A.; Jaffe, J. D.; Maccoss, M. J.; Maclean, B. Panorama: A Targeted Proteomics Knowledge Base. *J. Proteome Res.* **2014**, *13*, 4205−4210.
(57) Smyth, G. K. Linear Models and Empirical Bayes Methods for Assessing Differential Expression in Microarray Experiments. *Stat. Appl. Genet. Mol. Biol.* **2004**, *3*, 1−25.
(58) Chou, M. F.; Schwartz, D. Biological Sequence Motif Discovery Using Motif-X. *Curr. Protoc. Bioinf.* **2011**, *35*, 13.15.1−13.15.24.
(59) Schwartz, D.; Gygi, S. P. An Iterative Statistical Approach to the Identification of Protein Phosphorylation Motifs from Large-Scale Data Sets. *Nat. Biotechnol.* **2005**, *23*, 1391−1398.
(60) Tareen, A.; Kinney, J. B. Logomaker: Beautiful Sequence Logos in Python. *Bioinformatics* **2020**, *36*, 2272−2274.
(61) Wiredja, D. D.; Koyutürk, M.; Chance, M. R. The KSEA App: A Web-Based Tool for Kinase Activity Inference from Quantitative Phosphoproteomics. *Bioinformatics* **2017**, *33*, 3489−3491.
(62) Casado, P.; Rodriguez-Prados, J.-C.; Cosulich, S. C.; Guichard, S.; Vanhaesebroeck, B.; Joel, S.; Cutillas, P. R. Kinase-Substrate Enrichment Analysis Provides Insights into the Heterogeneity of Signaling Pathway Activation in Leukemia Cells. *Sci. Signaling* **2013**, *6*, No. rs6.
(63) Hornbeck, P. V.; Zhang, B.; Murray, B.; Kornhauser, J. M.; Latham, V.; Skrzypek, E. PhosphoSitePlus, 2014: Mutations, PTMs and Recalibrations. *Nucleic Acids Res.* **2015**, *43*, D512−D520.
(64) Ward, J. H. Hierarchical Grouping to Optimize an Objective Function. *J. Am. Stat. Assoc.* **1963**, *58*, 236.
(65) Virtanen, P.; Gommers, R.; Oliphant, T. E.; Haberland, M.; Reddy, T.; Cournapeau, D.; Burovski, E.; Peterson, P.; Weckesser, W.; Bright, J.; van der Walt, S. J.; Brett, M.; Wilson, J.; Millman, K. J.; Mayorov, N.; Nelson, A. R. J.; Jones, E.; Kern, R.; Larson, E.; Carey, C. J.; Polat, İ.; Feng, Y.; Moore, E. W.; VanderPlas, J.; Laxalde, D.; Perktold, J.; Cimrman, R.; Henriksen, I.; Quintero, E. A.; Harris, C. R.; Archibald, A. M.; Ribeiro, A. H.; Pedregosa, F.; van Mulbregt, P.; Vijaykumar, A.; Bardelli, A.; Pietro; Rothberg, A.; Hilboll, A.; Kloeckner, A.; Scopatz, A.; Lee, A.; Rokem, A.; Woods, C. N.; Fulton, C.; Masson, C.; Häggström, C.; Fitzgerald, C.; Nicholson, D. A.; Hagen, D. R.; Pasechnik, D. V.; Olivetti, E.; Martin, E.; Wieser, E.; Silva, F.; Lenders, F.; Wilhelm, F.; Young, G.; Price, G. A.; Ingold, G. L.; Allen, G. E.; Lee, G. R.; Audren, H.; Probst, I.; Dietrich, J. P.; Silterra, J.; Webber, J. T.; Slavič, J.; Nothman, J.; Buchner, J.; Kulick, J.; Schönberger, J. L.; de Miranda Cardoso, J. V.; Reimer, J.; Harrington, J.; Rodríguez, J. L. C.; Nunez-Iglesias, J.; Kuczynski, J.; Tritz, K.; Thoma, M.; Newville, M.; Kümmerer, M.; Bolingbroke, M.; Tartre, M.; Pak, M.; Smith, N. J.; Nowaczyk, N.; Shebanov, N.; Pavlyk, O.; Brodtkorb, P. A.; Lee, P.; McGibbon, R. T.; Feldbauer, R.; Lewis, S.; Tygier, S.; Sievert, S.; Vigna, S.; Peterson, S.; More, S.; Pudlik, T.; Oshima, T.; Pingel, T. J.; Robitaille, T. P.; Spura, T.; Jones, T. R.; Cera, T.; Leslie, T.; Zito, T.; Krauss, T.; Upadhyay, U.; Halchenko, Y. O.; Vázquez-Baeza, Y.; SciPy 1.0 Contributors. SciPy 1.0: Fundamental Algorithms for Scientific Computing in Python. *Nat. Methods* **2020**, *17*, 261−272.
(66) Johnson, M.; Zaretskaya, I.; Raytselis, Y.; Merezhuk, Y.; McGinnis, S.; Madden, T. L. NCBI BLAST: A Better Web Interface. *Nucleic Acids Res.* **2008**, *36*, W5−W9.
(67) UniProt Consortium; Bateman, A.; Martin, M. J.; et al. UniProt: The Universal Protein Knowledgebase in 2021. *Nucleic Acids Res.* **2021**, *49*, D480−D489.
(68) Cock, P. J. A.; Antao, T.; Chang, J. T.; Chapman, B. A.; Cox, C. J.; Dalke, A.; Friedberg, I.; Hamelryck, T.; Kauff, F.; Wilczynski, B.; de Hoon, M. J. L. Biopython: Freely Available Python Tools for

https://doi.org/10.1021/acs.jproteome.2c00505
J. Proteome Res. XXXX, XXX, XXX−XXX

Computational Molecular Biology and Bioinformatics. *Bioinformatics* **2009**, *25*, 1422−1423.
(69) Szklarczyk, D.; Gable, A. L.; Lyon, D.; Junge, A.; Wyder, S.; Huerta-Cepas, J.; Simonovic, M.; Doncheva, N. T.; Morris, J. H.; Bork, P.; Jensen, L. J.; Von Mering, C. STRING V11: Protein-Protein Association Networks with Increased Coverage, Supporting Functional Discovery in Genome-Wide Experimental Datasets. *Nucleic Acids Res.* **2019**, *47*, D607−D613.
(70) Murray, J. T.; Campbell, D. G.; Peggie, M.; Alfonso, M.; Cohen, P. Identification of Filamin C as a New Physiological Substrate of PKBα Using KESTREL. *Biochem. J.* **2004**, *384*, 489−494.
(71) Wang, L.; Harris, T. E.; Lawrence, J. C. Regulation of Proline-Rich Akt Substrate of 40 KDa (PRAS40) Function by Mammalian Target of Rapamycin Complex 1 (MTORC1)-Mediated Phosphorylation. *J. Biol. Chem.* **2008**, *283*, 15619−15627.
(72) Brunn, G. J.; Williams, J.; Sabers, C.; Wiederrecht, G.; Lawrence, J. C.; Abraham, R. T. Direct Inhibition of the Signaling Functions of the Mammalian Target of Rapamycin by the Phosphoinositide 3-Kinase Inhibitors, Wortmannin and LY294002. *EMBO J.* **1996**, *15*, 5256−5267.
(73) Gharbi, S. I.; Zvelebil, M. J.; Shuttleworth, S. J.; Hancox, T.; Saghir, N.; Timms, J. F.; Waterfield, M. D. Exploring the Specificity of the PI3K Family Inhibitor LY294002. *Biochem. J.* **2007**, *404*, 15−21.
(74) An, H.; Ordureau, A.; Paulo, J. A.; Shoemaker, C. J.; Denic, V.; Harper, J. W. TEX264 Is an Endoplasmic Reticulum-Resident ATG8-Interacting Protein Critical for ER Remodeling during Nutrient Stress. *Mol. Cell* **2019**, *74*, 891.e10−908.e10.
(75) Li, J.; Van Vranken, J. G.; Pontano Vaites, L.; Schweppe, D. K.; Huttlin, E. L.; Etienne, C.; Nandhikonda, P.; Viner, R.; Robitaille, A. M.; Thompson, A. H.; Kuhn, K.; Pike, I.; Bomgarden, R. D.; Rogers, J. C.; Gygi, S. P.; Paulo, J. A. TMTpro Reagents: A Set of Isobaric Labeling Mass Tags Enables Simultaneous Proteome-Wide Measurements Across 16 Samples. *Nat. Methods* **2020**, *17*, 399−404.
(76) Garbern, J. C.; Helman, A.; Sereda, R.; Sarikhani, M.; Ahmed, A.; Escalante, G. O.; Ogurlu, R.; Kim, S. L.; Zimmerman, J. F.; Cho, A.; MacQueen, L.; Bezzerides, V. J.; Parker, K. K.; Melton, D. A.; Lee, R. T. Inhibition of MTOR Signaling Enhances Maturation of Cardiomyocytes Derived from Human-Induced Pluripotent Stem Cells via P53-Induced Quiescence. *Circulation* **2020**, *141*, 285−300.
(77) Baffi, T. R.; Lordén, G.; Wozniak, J. M.; Feichtner, A.; Yeung, W.; Kornev, A. P.; King, C. C.; Del Rio, J. C.; Limaye, A. J.; Bogomolovas, J.; Gould, C. M.; Chen, J.; Kennedy, E. J.; Kannan, N.; Gonzalez, D. J.; Stefan, E.; Taylor, S. S.; Newton, A. C. MTORC2 Controls the Activity of PKC and Akt by Phosphorylating a Conserved TOR Interaction Motif. *Sci. Signaling* **2021**, *14*, No. eabe4509.
(78) Liu, Q.; Kirubakaran, S.; Hur, W.; Niepel, M.; Westover, K.; Thoreen, C. C.; Wang, J.; Ni, J.; Patricelli, M. P.; Vogel, K.; Riddle, S.; Waller, D. L.; Traynor, R.; Sanda, T.; Zhao, Z.; Kang, S. A.; Zhao, J.; Look, A. T.; Sorger, P. K.; Sabatini, D. M.; Gray, N. S. Kinome-Wide Selectivity Profiling of ATP-Competitive Mammalian Target of Rapamycin (MTOR) Inhibitors and Characterization of Their Binding Kinetics. *J. Biol. Chem.* **2012**, *287*, 9742−9752.
(79) Humphrey, S. J.; Yang, G.; Yang, P.; Fazakerley, D. J.; Stöckli, J.; Yang, J. Y.; James, D. E. Dynamic Adipocyte Phosphoproteome Reveals That Akt Directly Regulates MTORC2. *Cell Metab.* **2013**, *17*, 1009−1020.
(80) Yang, G.; Murashige, D. S.; Humphrey, S. J.; James, D. E. A Positive Feedback Loop between Akt and MTORC2 via SIN1 Phosphorylation. *Cell Rep.* **2015**, *12*, 937−943.
(81) Magnusson, R.; Gustafsson, M.; Cedersund, G.; Strålfors, P.; Nyman, E. Cross-Talks via MTORC2 Can Explain Enhanced Activation in Response to Insulin in Diabetic Patients. *Biosci. Rep.* **2017**, *37*, No. BSR20160514.
(82) Thoreen, C. C.; Kang, S. A.; Chang, J. W.; Liu, Q.; Zhang, J.; Gao, Y.; Reichling, L. J.; Sim, T.; Sabatini, D. M.; Gray, N. S. An ATP-Competitive Mammalian Target of Rapamycin Inhibitor Reveals Rapamycin-Resistant Functions of MTORC1. *J. Biol. Chem.* **2009**, *284*, 8023−8032.
(83) Altomare, D. A.; Lyons, G. E.; Mitsuuchi, Y.; Cheng, J. Q.; Testa, J. R. Akt2 MRNA Is Highly Expressed in Embryonic Brown Fat and the AKT2 Kinase Is Activated by Insulin. *Oncogene* **1998**, *16*, 2407−2411.
(84) Cho, H.; Mu, J.; Kim, J. K.; Thorvaldsen, J. L.; Chu, Q.; Crenshaw, E. B.; Kaestner, K. H.; Bartolomei, M. S.; Shulman, G. I.; Birnbaum, M. J. Insulin Resistance and a Diabetes Mellitus-Like Syndrome in Mice Lacking the Protein Kinase Akt2 (PKB Beta). *Science* **2001**, *292*, 1728−1731.
(85) Garofalo, R. S.; Orena, S. J.; Rafidi, K.; Torchia, A. J.; Stock, J. L.; Hildebrandt, A. L.; Coskran, T.; Black, S. C.; Brees, D. J.; Wicks, J. R.; McNeish, J. D.; Coleman, K. G. Severe Diabetes, Age-Dependent Loss of Adipose Tissue, and Mild Growth Deficiency in Mice Lacking Akt2/PKBβ. *J. Clin. Invest.* **2003**, *112*, 197−208.
(86) Chen, W. S.; Xu, P.; Gottlob, K.; Chen, M.; Sokol, K.; Shiyanova, T.; Roninson, I.; Weng, W.; Suzuki, R.; Tobe, K.; Kadowaki, T.; Hay, N. Growth Retardation and Increased Apoptosis in Mice with Homozygous Disruption of the Akt1 Gene. *Genes Dev.* **2001**, *15*, 2203−2208.
(87) Cho, H.; Thorvaldsen, J. L.; Chu, Q.; Feng, F.; Birnbaum, M. J. Akt1/PKBα Is Required for Normal Growth but Dispensable for Maintenance of Glucose Homeostasis in Mice. *J. Biol. Chem.* **2001**, *276*, 38349−38352.
(88) Brodbeck, D.; Cron, P.; Hemmings, B. A. A Human Protein Kinase Bγ with Regulatory Phosphorylation Sites in the Activation Loop and in the C-Terminal Hydrophobic Domain. *J. Biol. Chem.* **1999**, *274*, 9133−9136.
(89) Nakatani, K.; Sakaue, H.; Thompson, D. A.; Weigel, R. J.; Roth, R. A. Identification of a Human Akt3 (Protein Kinase B γ) Which Contains the Regulatory Serine Phosphorylation Site. *Biochem. Biophys. Res. Commun.* **1999**, *257*, 906−910.
(90) Gout, I.; Minami, T.; Hara, K.; Tsujishita, Y.; Filonenko, V.; Waterfield, M. D.; Yonezawa, K. Molecular Cloning and Characterization of a Novel P70 S6 Kinase, P70 S6 Kinase β Containing a Proline-Rich Region. *J. Biol. Chem.* **1998**, *273*, 30061−30064.
(91) Shima, H.; Pende, M.; Chen, Y.; Fumagalli, S.; Thomas, G.; Kozma, S. C. Disruption of the P70s6k/P85s6k Gene Reveals a Small Mouse Phenotype and a New Functional S6 Kinase. *EMBO J.* **1998**, *17*, 6649−6659.
(92) Marabita, M.; Baraldo, M.; Solagna, F.; Ceelen, J. J. M.; Sartori, R.; Nolte, H.; Nemazanyy, I.; Pyronnet, S.; Kruger, M.; Pende, M.; Blaauw, B. S6K1 Is Required for Increasing Skeletal Muscle Force during Hypertrophy. *Cell Rep.* **2016**, *17*, 501−513.
(93) Moller, D. E.; Xia, C. H.; Tang, W.; Zhu, A. X.; Jakubowski, M. Human Rsk Isoforms: Cloning and Characterization of Tissue-Specific Expression. *Am. J. Physiol.: Cell Physiol.* **1994**, *266*, C351−C359.
(94) Zeniou, M.; Ding, T.; Trivier, E.; Hanauer, A. Expression Analysis of RSK Gene Family Members: The RSK2 Gene, Mutated in Coffin-Lowry Syndrome, Is Prominently Expressed in Brain Structures Essential for Cognitive Function and Learning. *Hum. Mol. Genet.* **2002**, *11*, 2929−2940.
(95) Leighton, I. A.; Dalby, K. N.; Barry Caudwell, F.; Cohen, P. T. W.; Cohen, P. Comparison of the Specificities of P70 S6 Kinase and MAPKAP Kinase-1 Identifies a Relatively Specific Substrate for P70 S6 Kinase: The N-Terminal Kinase Domain of MAPKAP Kinase-1 Is Essential for Peptide Phosphorylation. *FEBS Lett.* **1995**, *375*, 289−293.
(96) Shabb, J. B. Physiological Substrates of CAMP-Dependent Protein Kinase. *Chem. Rev.* **2001**, *101*, 2381−2412.
(97) Smith, F. D.; Samelson, B. K.; Scott, J. D. Discovery of Cellular Substrates for Protein Kinase A Using a Peptide Array Screening Protocol. *Biochem. J.* **2011**, *438*, 103−110.
(98) Méant, A.; Gao, B.; Lavoie, G.; Nourreddine, S.; Jung, F.; Aubert, L.; Tcherkezian, J.; Gingras, A.-C.; Roux, P. P. Proteomic Analysis Reveals a Role for RSK in P120-Catenin Phosphorylation and Melanoma Cell-Cell Adhesion. *Mol. Cell. Proteomics* **2020**, *19*, 50−64.
(99) Davies, S. P.; Reddy, H.; Caivano, M.; Cohen, P. Specificity and Mechanism of Action of Some Commonly Used Protein Kinase Inhibitors. *Biochem. J.* **2000**, *351*, 95.
(100) Jacobs, M. D.; Black, J.; Futer, O.; Swenson, L.; Hare, B.; Fleming, M.; Saxena, K. Pim-1 Ligand-Bound Structures Reveal the

https://doi.org/10.1021/acs.jproteome.2c00505
J. Proteome Res. XXXX, XXX, XXX−XXX

Mechanism of Serine/Threonine Kinase Inhibition by LY294002. *J. Biol. Chem.* **2005**, *280*, 13728−13734.
(101) Song, J. H.; Padi, S. K. R.; Luevano, L. A.; Minden, M. D.; DeAngelo, D. J.; Hardiman, G.; Ball, L. E.; Warfel, N. A.; Kraft, A. S. Insulin Receptor Substrate 1 Is a Substrate of the Pim Protein Kinases. *Oncotarget* **2016**, *7*, 20152−20165.
(102) Liu, X.; Xiao, W.; Zhang, Y.; Wiley, S. E.; Zuo, T.; Zheng, Y.; Chen, N.; Chen, L.; Wang, X.; Zheng, Y.; Huang, L.; Lin, S.; Murphy, A. N.; Dixon, J. E.; Xu, P.; Guo, X. Reversible Phosphorylation of Rpn1 Regulates 26S Proteasome Assembly and Function. *Proc. Natl. Acad. Sci. U.S.A.* **2020**, *117*, 328−336.
(103) Wang, C.; Ye, M.; Bian, Y.; Liu, F.; Cheng, K.; Dong, M.; Dong, J.; Zou, H. Determination of CK2 Specificity and Substrates by Proteome-Derived Peptide Libraries. *J. Proteome Res.* **2013**, *12*, 3813−3821.
(104) Rusin, S. F.; Adamo, M. E.; Kettenbach, A. N. Identification of Candidate Casein Kinase 2 Substrates in Mitosis by Quantitative Phosphoproteomics. *Front. Cell Dev. Biol.* **2017**, *5*, No. 97.
(105) Kim, S. T.; Lim, D. S.; Canman, C. E.; Kastan, M. B. Substrate Specificities and Identification of Putative Substrates of ATM Kinase Family Members. *J. Biol. Chem.* **1999**, *274*, 37538−37543.
(106) King, W. G.; Mattaliano, M. D.; Chan, T. O.; Tsichlis, P. N.; Brugge, J. S. Phosphatidylinositol 3-Kinase Is Required for Integrin-Stimulated AKT and Raf-1/Mitogen-Activated Protein Kinase Pathway Activation. *Mol. Cell. Biol.* **1997**, *17*, 4406−4418.
(107) Grandage, V. L.; Gale, R. E.; Lich, D. C.; Khwaja, A. PI3-Kinase/Akt Is Constitutively Active in Primary Acute Myeloid Leukaemia Cells and Regulates Survival and Chemoresistance via NF-KB, MAPkinase and P53 Pathways. *Leukemia* **2005**, *19*, 586−594.
(108) Ebi, H.; Costa, C.; Faber, A. C.; Nishtala, M.; Kotani, H.; Juric, D.; Della Pelle, P.; Song, Y.; Yano, S.; Mino-Kenudson, M.; Benes, C. H.; Engelman, J. A. PI3K Regulates MEK/ERK Signaling in Breast Cancer via the Rac-GEF, P-Rex1. *Proc. Natl. Acad. Sci. U.S.A.* **2013**, *110*, 21124−21129.
(109) Duff, A.; Kavege, L.; Baquier, J.; Hu, T. A PI3K Inhibitor-Induced Growth Inhibition of Cancer Cells Is Linked to MEK-ERK Pathway. *Anti-Cancer Drugs* **2021**, *32*, 517−525.
(110) Fey, D.; Croucher, D. R.; Kolch, W.; Kholodenko, B. N. Crosstalk and Signaling Switches in Mitogen-Activated Protein Kinase Cascades. *Front. Physiol.* **2012**, *3*, No. 355.
(111) Dokladda, K.; Green, K. A.; Pan, D. A.; Hardie, D. G. PD98059 and U0126 Activate AMP-Activated Protein Kinase by Increasing the Cellular AMP:ATP Ratio and Not Via Inhibition of the MAP Kinase Pathway. *FEBS Lett.* **2005**, *579*, 236−240.
(112) Hefner, Y.; Borsch-Haubold, A. G.; Murakami, M.; Wilde, J. I.; Pasquet, S.; Schieltz, D.; Ghomashchi, F.; Yates, J. R.; Armstrong, C. G.; Paterson, A.; Cohen, P.; Fukunaga, R.; Hunter, T.; Kudo, I.; Watson, S. P.; Gelb, M. H. Serine 727 Phosphorylation and Activation of Cytosolic Phospholipase A2 by MNK1-Related Protein Kinases. *J. Biol. Chem.* **2000**, *275*, 37542−37551.
(113) Shum, M.; Houde, V. P.; Bellemare, V.; Moreira, R. J.; Bellmann, K.; St-Pierre, P.; Viollet, B.; Foretz, M.; Marette, A. Inhibition of Mitochondrial Complex 1 by the S6K1 Inhibitor PF-4708671 Partly Contributes to Its Glucose Metabolic Effects in Muscle and Liver Cells. *J. Biol. Chem.* **2019**, *294*, 12250−12260.
(114) Nishimura, Y.; Chunthorng-Orn, J.; Lord, S.; Musa, I.; Dawson, P.; Holm, L.; Lai, Y.-C. Ubiquitin E3 Ligase Atrogin-1 Protein Is Regulated via the Rapamycin-Sensitive MTOR-S6K1 Signaling Pathway in C2C12 Muscle Cells. *Am. J. Physiol.: Cell Physiol.* **2022**, *323*, C215−C225.
(115) Needham, E. J.; Hingst, J. R.; Parker, B. L.; Morrison, K. R.; Yang, G.; Onslev, J.; Kristensen, J. M.; Højlund, K.; Ling, N. X. Y.; Oakhill, J. S.; Richter, E. A.; Kiens, B.; Petersen, J.; Pehmøller, C.; James, D. E.; Wojtaszewski, J. F. P.; Humphrey, S. J. Personalized Phosphoproteomics Identifies Functional Signaling. *Nat. Biotechnol.* **2022**, *40*, 576−584.
(116) Sapkota, G. P.; Cummings, L.; Newell, F. S.; Armstrong, C.; Bain, J.; Frodin, M.; Grauert, M.; Hoffmann, M.; Schnapp, G.; Steegmaier, M.; Cohen, P.; Alessi, D. R. BI-D1870 Is a Specific Inhibitor of the P90 RSK (Ribosomal S6 Kinase) Isoforms In Vitro and In Vivo. *Biochem. J.* **2007**, *401*, 29−38.
(117) Fonseca, B. D.; Alain, T.; Finestone, L. K.; Huang, B. P. H.; Rolfe, M.; Jiang, T.; Yao, Z.; Hernandez, G.; Bennett, C. F.; Proud, C. G. Pharmacological and Genetic Evaluation of Proposed Roles of Mitogen-Activated Protein Kinase/Extracellular Signal-Regulated Kinase Kinase (MEK), Extracellular Signal-Regulated Kinase (ERK), and P90RSK in the Control of MTORC1 Protein Signaling by Phorbol. *J. Biol. Chem.* **2011**, *286*, 27111−27122.
(118) Errico, A.; Deshmukh, K.; Tanaka, Y.; Pozniakovsky, A.; Hunt, T. Identification of Substrates for Cyclin Dependent Kinases. *Adv. Enzyme Regul.* **2010**, *50*, 375−399.
(119) Wiechmann, S.; Ruprecht, B.; Siekmann, T.; Zheng, R.; Frejno, M.; Kunold, E.; Bajaj, T.; Zolg, D. P.; Sieber, S. A.; Gassen, N. C.; Kuster, B. Chemical Phosphoproteomics Sheds New Light on the Targets and Modes of Action of AKT Inhibitors. *ACS Chem. Biol.* **2021**, *16*, 631−641.
(120) Nishi, H.; Demir, E.; Panchenko, A. R. Crosstalk between Signaling Pathways Provided by Single and Multiple Protein Phosphorylation Sites. *J. Mol. Biol.* **2015**, *427*, 511−520.
(121) Blangy, A. Tensins Are Versatile Regulators of Rho GTPase Signalling and Cell Adhesion. *Biol. Cell* **2017**, *109*, 115−126.
(122) Maruyama, K. Connectin/Titin, Giant Elastic Protein of Muscle. *FASEB J.* **1997**, *11*, 341−345.
(123) Linke, W. A. Titin Gene and Protein Functions in Passive and Active Muscle. *Annu. Rev. Physiol.* **2018**, *80*, 389−411.
(124) Konieczny, P.; Fuchs, P.; Reipert, S.; Kunz, W. S.; Zeöld, A.; Fischer, I.; Paulin, D.; Schröder, R.; Wiche, G. Myofiber Integrity Depends on Desmin Network Targeting to Z-Disks and Costameres via Distinct Plectin Isoforms. *J. Cell Biol.* **2008**, *181*, 667−681.
(125) Dedeic, Z.; Cetera, M.; Cohen, T. V.; Holaska, J. M. Emerin Inhibits Lmo7 Binding to the Pax3 and MyoD Promoters and Expression of Myoblast Proliferation Genes. *J. Cell Sci.* **2011**, *124*, 1691−1702.
(126) Hashimoto, Y.; Kinoshita, N.; Greco, T. M.; Federspiel, J. D.; Jean Beltran, P. M.; Ueno, N.; Cristea, I. M. Mechanical Force Induces Phosphorylation-Mediated Signaling That Underlies Tissue Response and Robustness in Xenopus Embryos. *Cell Syst.* **2019**, *8*, 226.e7−241.e7.
(127) Anderson, D. M.; Cannavino, J.; Li, H.; Anderson, K. M.; Nelson, B. R.; McAnally, J.; Bezprozvannaya, S.; Liu, Y.; Lin, W.; Liu, N.; Bassel-Duby, R.; Olson, E. N. Severe Muscle Wasting and Denervation in Mice Lacking the RNA-Binding Protein ZFP106. *Proc. Natl. Acad. Sci. U.S.A.* **2016**, *113*, E4494−E4503.
(128) Fero, K.; Bergeron, S. A.; Horstick, E. J.; Codore, H.; Li, G. H.; Ono, F.; Dowling, J. J.; Burgess, H. A. Impaired Embryonic Motility in Dusp27 Mutants Reveals a Developmental Defect in Myofibril Structure. *Dis. Models Mech.* **2013**, *7*, 289−298.
(129) Mayo, L. D.; Donner, D. B. A Phosphatidylinositol 3-Kinase/Akt Pathway Promotes Translocation of Mdm2 from the Cytoplasm to the Nucleus. *Proc. Natl. Acad. Sci. U.S.A.* **2001**, *98*, 11598−11603.
(130) Ogawara, Y.; Kishishita, S.; Obata, T.; Isazawa, Y.; Suzuki, T.; Tanaka, K.; Masuyama, N.; Gotoh, Y. Akt Enhances Mdm2-Mediated Ubiquitination and Degradation of P53. *J. Biol. Chem.* **2002**, *277*, 21843−21850.
(131) Zhou, B. P.; Liao, Y.; Xia, W.; Zou, Y.; Spohn, B.; Hung, M. HER-2/Neu Induces P53 Ubiquitination via Akt-Mediated MDM2 Phosphorylation. *Nat. Cell Biol.* **2001**, *3*, 973−982.
(132) Arena, G.; Cissé, M. Y.; Pyrdziak, S.; Chatre, L.; Riscal, R.; Fuentes, M.; Arnold, J. J.; Kastner, M.; Gayte, L.; Bertrand-Gaday, C.; Nay, K.; Angebault-Prouteau, C.; Murray, K.; Chabi, B.; Koechlin-Ramonatxo, C.; Orsetti, B.; Vincent, C.; Casas, F.; Marine, J.-C.; Etienne-Manneville, S.; Bernex, F.; Lombès, A.; Cameron, C. E.; Dubouchaud, H.; Ricchetti, M.; Linares, L. K.; Le Cam, L. Mitochondrial MDM2 Regulates Respiratory Complex I Activity Independently of P53. *Mol. Cell* **2018**, *69*, 594.e8−609.e8.
(133) He, M. Y.; Xu, S. B.; Qu, Z. H.; Guo, Y. M.; Liu, X. C.; Cong, X. X.; Wang, J. F.; Low, B. C.; Li, L.; Wu, Q.; Lin, P.; Yan, S. G.; Bao, Z.; Zhou, Y. T.; Zheng, L. L. Hsp90β Interacts with MDM2 to Suppress

https://doi.org/10.1021/acs.jproteome.2c00505
J. Proteome Res. XXXX, XXX, XXX−XXX

P53-dependent Senescence during Skeletal Muscle Regeneration. *Aging Cell* **2019**, *18*, No. e13003.
(134) Roudier, E.; Forn, P.; Perry, M. E.; Birot, O. Murine Double Minute-2 Expression Is Required for Capillary Maintenance and Exercise-Induced Angiogenesis in Skeletal Muscle. *FASEB J.* **2012**, *26*, 4530−4539.
(135) Elkholi, R.; Abraham-Enachescu, I.; Trotta, A. P.; Rubio-Patiño, C.; Mohammed, J. N.; Luna-Vargas, M. P. A.; Gelles, J. D.; Kaminetsky, J. R.; Serasinghe, M. N.; Zou, C.; Ali, S.; McStay, G. P.; Pfleger, C. M.; Chipuk, J. E. MDM2 Integrates Cellular Respiration and Apoptotic Signaling through NDUFS1 and the Mitochondrial Network. *Mol. Cell* **2019**, *74*, 452.e7−465.e7.
(136) Hoffman, N. J.; Parker, B. L.; Chaudhuri, R.; Fisher-Wellman, K. H.; Kleinert, M.; Humphrey, S. J.; Yang, P.; Holliday, M.; Trefely, S.; Fazakerley, D. J.; Stöckli, J.; Burchfield, J. G.; Jensen, T. E.; Jothi, R.; Kiens, B.; Wojtaszewski, J. F. P.; Richter, E. A.; James, D. E. Global Phosphoproteomic Analysis of Human Skeletal Muscle Reveals a Network of Exercise-Regulated Kinases and AMPK Substrates. *Cell Metab.* **2015**, *22*, 922−935.
(137) Qi, B.; He, L.; Zhao, Y.; Zhang, L.; He, Y.; Li, J.; Li, C.; Zhang, B.; Huang, Q.; Xing, J.; Li, F.; Li, Y.; Ji, L. Akap1 Deficiency Exacerbates Diabetic Cardiomyopathy in Mice by NDUFS1-Mediated Mitochondrial Dysfunction and Apoptosis. *Diabetologia* **2020**, *63*, 1072−1087.
(138) Beqqali, A.; Monshouwer-Kloots, J.; Monteiro, R.; Welling, M.; Bakkers, J.; Ehler, E.; Verkleij, A.; Mummery, C.; Passier, R. CHAP Is a Newly Identified Z-Disc Protein Essential for Heart and Skeletal Muscle Function. *J. Cell Sci.* **2010**, *123*, 1141−1150.
(139) Henderson, C. A.; Gomez, C. G.; Novak, S. M.; Mi-Mi, L.; Gregorio, C. C. Overview of the Muscle Cytoskeleton. In *Comprehensive Physiology*; Wiley, 2017; Vol. 7, pp 891−944.
(140) Clark, K. A.; McElhinny, A. S.; Beckerle, M. C.; Gregorio, C. C. Striated Muscle Cytoarchitecture: An Intricate Web of Form and Function. *Annu. Rev. Cell Dev. Biol.* **2002**, *18*, 637−706.
(141) Clarkson, E.; Costa, C. F.; Machesky, L. M. Congenital Myopathies: Diseases of the Actin Cytoskeleton. *J. Pathol.* **2004**, *204*, 407−417.
(142) Yoshizaki, T.; Imamura, T.; Babendure, J. L.; Lu, J.-C.; Sonoda, N.; Olefsky, J. M. Myosin 5a Is an Insulin-Stimulated Akt2 (Protein Kinase Bβ) Substrate Modulating GLUT4 Vesicle Translocation. *Mol. Cell. Biol.* **2007**, *27*, 5172−5183.
(143) Smadja-Lamère, N.; Shum, M.; Déléris, P.; Roux, P. P.; Abe, J.-I.; Marette, A. Insulin Activates RSK (P90 Ribosomal S6 Kinase) to Trigger a New Negative Feedback Loop That Regulates Insulin Signaling for Glucose Metabolism. *J. Biol. Chem.* **2013**, *288*, 31165−31176.
(144) Becker, R.; Leone, M.; Engel, F. Microtubule Organization in Striated Muscle Cells. *Cells* **2020**, *9*, No. 1395.
(145) Jabre, S.; Hleihel, W.; Coirault, C. Nuclear Mechanotransduction in Skeletal Muscle. *Cells* **2021**, *10*, No. 318.
(146) Du, Q.; Taylor, L.; Compton, D. A.; Macara, I. G. LGN Blocks the Ability of NuMA to Bind and Stabilize Microtubules. *Curr. Biol.* **2002**, *12*, 1928−1933.
(147) Welburn, J. P. I.; Cheeseman, I. M. The Microtubule-Binding Protein Cep170 Promotes the Targeting of the Kinesin-13 Depolymerase Kif2b to the Mitotic Spindle. *Mol. Biol. Cell* **2012**, *23*, 4786−4795.
(148) Wu, X.; Kodama, A.; Fuchs, E. ACF7 Regulates Cytoskeletal-Focal Adhesion Dynamics and Migration and Has ATPase Activity. *Cell* **2008**, *135*, 137−148.
(149) Saadi, I.; Alkuraya, F. S.; Gisselbrecht, S. S.; Goessling, W.; Cavallesco, R.; Turbe-Doan, A.; Petrin, A. L.; Harris, J.; Siddiqui, U.; Grix, A. W.; Hove, H. D.; Leboulch, P.; Glover, T. W.; Morton, C. C.; Richieri-Costa, A.; Murray, J. C.; Erickson, R. P.; Maas, R. L. Deficiency of the Cytoskeletal Protein SPECC1L Leads to Oblique Facial Clefting. *Am. J. Hum. Genet.* **2011**, *89*, 44−55.
(150) Bernier, G.; Pool, M.; Kilcup, M.; Alfoldi, J.; De Repentigny, Y.; Kothary, R. Acf7 (MACF) Is an Actin and Microtubule Linker Protein Whose Expression Predominates in Neural, Muscle, and Lung Development. *Dev. Dyn.* **2000**, *219*, 216−225.
(151) Oury, J.; Liu, Y.; Töpf, A.; Todorovic, S.; Hoedt, E.; Preethish-Kumar, V.; Neubert, T. A.; Lin, W.; Lochmüller, H.; Burden, S. J. MACF1 Links Rapsyn to Microtubule- and Actin-Binding Proteins to Maintain Neuromuscular Synapses. *J. Cell Biol.* **2019**, *218*, 1686−1705.
(152) Lumeng, C.; Phelps, S.; Crawford, G. E.; Walden, P. D.; Barald, K.; Chamberlain, J. S. Interactions between B2-Syntrophin and a Family of Microtubule-Associated Serine/Threonine Kinases. *Nat. Neurosci.* **1999**, *2*, 611−617.
(153) Hotta, A.; Kawakatsu, T.; Nakatani, T.; Sato, T.; Matsui, C.; Sukezane, T.; Akagi, T.; Hamaji, T.; Grigoriev, I.; Akhmanova, A.; Takai, Y.; Mimori-Kiyosue, Y. Laminin-Based Cell Adhesion Anchors Microtubule plus Ends to the Epithelial Cell Basal Cortex through LL5α/β. *J. Cell Biol.* **2010**, *189*, 901−917.
(154) Astro, V.; Chiaretti, S.; Magistrati, E.; Fivaz, M.; de Curtis, I. Liprin-A1, ERC1 and LL5 Identify a Polarized, Dynamic Compartment Implicated in Cell Migration. *J. Cell Sci.* **2014**, *127*, 3862−3876.
(155) Zhou, Q. L.; Jiang, Z. Y.; Mabardy, A. S.; Del Campo, C. M.; Lambright, D. G.; Holik, J.; Fogarty, K. E.; Straubhaar, J.; Nicoloro, S.; Chawla, A.; Czech, M. P. A Novel Pleckstrin Homology Domain-Containing Protein Enhances Insulin-Stimulated Akt Phosphorylation and GLUT4 Translocation in Adipocytes. *J. Biol. Chem.* **2010**, *285*, 27581−27589.
(156) Lansbergen, G.; Grigoriev, I.; Mimori-Kiyosue, Y.; Ohtsuka, T.; Higa, S.; Kitajima, I.; Demmers, J.; Galjart, N.; Houtsmuller, A. B.; Grosveld, F.; Akhmanova, A. CLASPs Attach Microtubule Plus Ends to the Cell Cortex through a Complex with LL5β. *Dev. Cell* **2006**, *11*, 21−32.
(157) Furu, M.; Kajita, Y.; Nagayama, S.; Ishibe, T.; Shima, Y.; Nishijo, K.; Uejima, D.; Takahashi, R.; Aoyama, T.; Nakayama, T.; Nakamura, T.; Nakashima, Y.; Ikegawa, M.; Imoto, S.; Katagiri, T.; Nakamura, Y.; Toguchida, J. Identification of AFAP1L1 as a Prognostic Marker for Spindle Cell Sarcomas. *Oncogene* **2011**, *30*, 4015−4025.
(158) Takahashi, R.; Nagayama, S.; Furu, M.; Kajita, Y.; Jin, Y.; Kato, T.; Imoto, S.; Sakai, Y.; Toguchida, J. AFAP1L1, a Novel Associating Partner with Vinculin, Modulates Cellular Morphology and Motility, and Promotes the Progression of Colorectal Cancers. *Cancer Med.* **2014**, *3*, 759−774.
(159) Chen, R. H.; Sarnecki, C.; Blenis, J. Nuclear Localization and Regulation of Erk- and Rsk-Encoded Protein Kinases. *Mol. Cell. Biol.* **1992**, *12*, 915−927.
(160) Ching, Y.-P.; Wong, C.-M.; Chan, S.-F.; Leung, T. H.-Y.; Ng, D. C.-H.; Jin, D.-Y.; Ng, I. O. Deleted in Liver Cancer (DLC) 2 Encodes a RhoGAP Protein with Growth Suppressor Function and Is Underexpressed in Hepatocellular Carcinoma. *J. Biol. Chem.* **2003**, *278*, 10824−10830.
(161) Bacon, C.; Endris, V.; Rappold, G. A. The Cellular Function of SrGAP3 and Its Role in Neuronal Morphogenesis. *Mech. Dev.* **2013**, *130*, 391−395.
(162) Jaafar, L.; Chamseddine, Z.; El-Sibai, M. StarD13: A Potential Star Target for Tumor Therapeutics. *Hum. Cell* **2020**, *33*, 437−443.
(163) Naumann, H.; Rathjen, T.; Poy, M. N.; Spagnoli, F. M. The RhoGAP Stard13 Controls Insulin Secretion through F-Actin Remodeling. *Mol. Metab.* **2018**, *8*, 96−105.
(164) Li, M.; Quan, C.; Toth, R.; Campbell, D. G.; MacKintosh, C.; Wang, H. Y.; Chen, S. Fasting and Systemic Insulin Signaling Regulate Phosphorylation of Brain Proteins That Modulate Cell Morphology and Link to Neurological Disorders. *J. Biol. Chem.* **2015**, *290*, 30030−30041.
(165) Kulasekaran, G.; Nossova, N.; Marat, A. L.; Lund, I.; Cremer, C.; Ioannou, M. S.; McPherson, P. S. Phosphorylation-Dependent Regulation of Connecdenn/DENND1 Guanine Nucleotide Exchange Factors. *J. Biol. Chem.* **2015**, *290*, 17999−18008.
(166) Nacke, M.; Sandilands, E.; Nikolatou, K.; Román-Fernández, Á.; Mason, S.; Patel, R.; Lilla, S.; Yelland, T.; Galbraith, L. C. A.; Freckmann, E. C.; McGarry, L.; Morton, J. P.; Shanks, E.; Leung, H. Y.; Markert, E.; Ismail, S.; Zanivan, S.; Blyth, K.; Bryant, D. M. An ARF GTPase Module Promoting Invasion and Metastasis through Regulating Phosphoinositide Metabolism. *Nat. Commun.* **2021**, *12*, No. 1623.

https://doi.org/10.1021/acs.jproteome.2c00505
J. Proteome Res. XXXX, XXX, XXX−XXX

(167) Malm, C.; Yu, J.-G. Exercise-Induced Muscle Damage and Inflammation: Re-Evaluation by Proteomics. *Histochem. Cell Biol.* **2012**, *138*, 89−99.
(168) Bei, Y.; Xu, T.; Lv, D.; Yu, P.; Xu, J.; Che, L.; Das, A.; Tigges, J.; Toxavidis, V.; Ghiran, I.; Shah, R.; Li, Y.; Zhang, Y.; Das, S.; Xiao, J. Exercise-Induced Circulating Extracellular Vesicles Protect against Cardiac Ischemia−Reperfusion Injury. *Basic Res. Cardiol.* **2017**, *112*, No. 38.
(169) D'Souza-Schorey, C.; Chavrier, P. ARF Proteins: Roles in Membrane Traffic and Beyond. *Nat. Rev. Mol. Cell Biol.* **2006**, *7*, 347−358.

https://doi.org/10.1021/acs.jproteome.2c00505
J. Proteome Res. XXXX, XXX, XXX−XXX